

JAAS

Accepted Manuscript



This is an *Accepted Manuscript*, which has been through the Royal Society of Chemistry peer review process and has been accepted for publication.

Accepted Manuscripts are published online shortly after acceptance, before technical editing, formatting and proof reading. Using this free service, authors can make their results available to the community, in citable form, before we publish the edited article. We will replace this *Accepted Manuscript* with the edited and formatted *Advance Article* as soon as it is available.

You can find more information about *Accepted Manuscripts* in the [Information for Authors](#).

Please note that technical editing may introduce minor changes to the text and/or graphics, which may alter content. The journal's standard [Terms & Conditions](#) and the [Ethical guidelines](#) still apply. In no event shall the Royal Society of Chemistry be held responsible for any errors or omissions in this *Accepted Manuscript* or any consequences arising from the use of any information it contains.

1
2
3 **Review of biological samples analysis using laser ablation inductively**
4 **coupled plasma mass spectrometry (LA-ICP-MS)**
5
6

7 **Dirce Pozebon,* Guilherme L. Scheffler,^a Valderi L. Dressler,^b and Matheus A.**
8 **G. Nunes^b**
9

10
11
12
13 *a: Instituto de Química, Universidade Federal do Rio grande do Sul, Av. Bento Gonçalves, 9500,*
14 *91.501-970, Porto Alegre, RS, Brazil*

15 *b: Departamento de Química, Universidade Federal de Santa Maria, Av. Roraima, 1000, 97.105-900*
16 *Santa Maria, RS, Brazil*
17
18
19
20
21
22
23
24
25
26
27
28
29
30
31
32
33
34
35
36
37
38
39
40
41
42
43
44
45
46
47
48
49
50
51
52
53

54 **To whom correspondence should be addressed (Dr. D. Pozebon):*
55 *dircepoz@iq.ufrgs.br*
56
57
58
59
60

Abstract

Laser ablation inductively coupled plasma mass spectrometry (LA-ICP-MS) has received significant attention over the last 10 years and has been widely used for analysis of biological samples. The technique allows elements and isotopes determination in biological tissues and related materials with a spatial resolution typically ranging from 10-100 μm . When compared to other techniques usually employed to obtain bioimages, the greater advantage of LA-ICP-MS is its higher sensitivity. The literature survey over the last 10 years concerning the use of LA-ICP-MS for biological tissues analysis is reviewed in this article. Instrumentation, strategies of calibration for quantitative analysis, challenges and recent advances in this field are discussed. Applications of isotope ratio (IR), including trace experiments, and isotope dilution (ID) are reviewed for biological samples (briefly for proteins, only in order to show the utility of LA-ICP-MS). Bioimaging methods, studies and applications to animal and plants tissues are emphasized, demonstrating the importance bioimage of metals and metalloids in biomedical research, bioaccumulation and bioavailability studies for ecological and toxicological risk assessment in humans, animals and plants. The usefulness of IR associated with bioimaging for predicting geographical origin, habitat, movement of subjects, diet and lifestyle are also demonstrated.

Introduction

Inductively coupled plasma mass spectrometry (ICP-MS) is recognized as a great analytical technique whose main features are large linear response, possibility of isotopic analysis, very low limit of detection (LOD) (in the range of ng L^{-1} for several elements) and multi-elemental capability. In addition, the ICP-ion source is extremely versatile to associate with different sample introduction systems, since the ICP accepts wet and dry aerosols and vapours. In addition to conventional pneumatic nebulization, which is the standard sample introduction method, electrothermal vaporization (ETV), direct injection nebulization (DIN), ultrasonic nebulization (USN), laser ablation (LA), and others can be associated with the ICP. The use of a specific sample introduction system can change considerable the response and capabilities of the ICP-MS technique, such as improvement of the LOD, reduction of spectral and non-spectral interferences, analysis of small sample amounts, reduction of sample handling and contamination. Laser ablation allows direct analysis of solids where the ablated material is carried to the ICP with the aid of a gas stream, usually Ar, Ar mixed with He or N_2 . Laser ablation is attractive, since it requires little or no sample preparation, offers good sample throughput, reduced spectral interferences and permits *in situ* analysis. Another important feature of LA is the high spatial resolution, normally at 10 - 100 μm for nanosecond (ns) laser. Higher spatial resolution ($< 1 \mu\text{m}$) is achieved using a femtosecond (fs) laser,¹ with low material uptake (in the μg order), making LA-ICP-MS as a quasi non-destructive technique. Better lateral resolution (at nm scale) was demonstrated by employing near field-LA-ICP-MS. However, this technique is still not mature deserving additional studies.²

From the time when LA-ICP-MS was introduced for solid sample analysis by Gray in 1985,³ the main challenge facing the technique application has been the possibility of fully quantitative analysis. Many efforts have been made to improve the LA-ICP-MS technique to achieve fully quantitative analysis, but this challenge still persists.⁴ The main reasons are non-stoichiometric effects occurring during sampling, aerosol transport, and vaporization, atomization and ionization within the ICP, which are the main negative effects. These phenomena are matrix-dependent and usually matrix matching standards (laboratory-produced or prepared with reference materials) are needed for quantitative analysis.

Since the early days of LA-ICP-MS, more than one hundred papers dealing with the technique application for biological tissues analysis have been published. The first

1
2
3 article describing the analysis of biological sample (certified reference materials) by
4 LA-ICP-MS was published by Durrant and Ward in 1992.⁵ The same authors⁶
5 reviewed the application of LA-ICP-MS to biological materials in 2005. The spatial
6 elemental distribution in biological tissues (bioimaging) by LA-ICP-MS was
7 introduced by Wang⁷ in 1994 and revisited by Kindness in 2003⁸. After that,
8 bioimaging researches and applications using LA-ICP-MS have grown substantially
9 with the pioneering effort of Becker,⁹⁻¹⁶ whereas a dedicated review was recently
10 published¹⁷. The use of LA-ICP-MS for biomedical applications, highlighting the
11 useful rank of the technique for early detection and treatment of diseases, especially
12 cancer and neurodegenerative ones, was reviewed by Konz *et al.*,¹⁸ in 2012.

13
14 The use of LA-ICP-MS for elemental analysis of biological tissues is reviewed in
15 the present article. The literature survey of the last 10 years was included. Topics of
16 particular interest include: instrumentation, which has great impact on the performance
17 and quality of data obtained by LA-ICP-MS, calibration strategies to obtain
18 quantitative information, isotope ratio in tracer experiments, and bioimaging, in which
19 LA-ICP-MS proved to be very useful. Only articles published in English have been
20 considered. “Bioimaging”, “Laser Ablation”, “LA-ICP-MS”, “Biological Tissues”,
21 “Animal Tissues”, “Plant Tissues”, “Bone and Teeth” and “Hair” are the keywords
22 used to do the revision. The authors apologize for any work not included in this review
23 article.

24 25 26 27 28 29 30 31 32 33 34 35 36 37 38 **Instrumentation**

39
40 Improvements of LA-ICP-MS have been achieved due to the rapid development of the laser
41 technology. Lasers with wavelength from infrared (IR) to ultraviolet (UV) have been
42 investigated for sample ablation and hyphenation with ICP-MS.¹⁹ A trend to change from
43 visible (694 nm and 532 nm) and IR (1064 nm) to UV wavelengths (266, 213 and 193 nm) is
44 observed; shorter wavelength lasers have demonstrated better ablation characteristics for
45 sample introduction in ICP-MS (see reference 19 and those cited therein). Different types of
46 laser instruments commonly used in the analysis of biological tissues as well as ICP-MS
47 instruments are exemplified in Table 1 (see further).

48
49 Elemental fractionation (sum of all non-stoichiometric effects during the ablation
50 process, aerosol transport and ionization in the ICP source) is one of the main
51 difficulties to obtain quantitative results in LA-ICP-MS. Many studies have been
52
53
54
55
56
57
58
59
60

1
2
3 dedicated to this topic, where various aspects of the technique were evaluated.²⁰⁻³¹
4 Laser wavelength, laser pulse duration, laser power and spot size are parameters that
5 influence on fractionation. Most of the studies about fractionation were conducted with
6 geological samples (mineral, oxides, silicates etc.) and metals or metal alloys, where
7 elemental fractionation is more pronounced. The absorption of the laser by oxides,
8 silicates and minerals seems to be the most important factor, whereas the ratio of the
9 signal intensity of different elements gradually changes over the course of the ablation
10 process, which depends on the type of material ablated. Based on these observations,
11 Fryer *et al.*⁴ and Longerich *et al.*³² calculated a relative fractionation index, which
12 allows classifying chemical elements into groups by considering similar behaviour
13 through ablation and ionization. Fractionation of U, Pb, Cu and Zn has been widely
14 studied as the fractionation index is very different for these elements.³³⁻³⁴ In general,
15 fractionation can be reduced by using shorter laser wavelength since thermal alteration
16 of the sample material is reduced with the laser wavelength decrease. For more
17 transparent materials to laser radiation, like silicates, the laser energy coupling into the
18 sample is improved, leading to higher energy densities. The increased interaction of the
19 laser radiation with the sample yields smaller ablation rate in transparent materials at a
20 given irradiance and reduces the heat transfer zone in the sample.^{25,35} Unlike the high-
21 transparency materials to laser radiation, the wavelength has less influence on
22 fractionation in metallic materials.²⁴ For such kind of materials the pulse duration
23 appears to be the dominant factor, which may lead to molten material around the
24 ablation spot, affecting the stoichiometry of the generated aerosol. This effect was
25 demonstrated by Poitrasson *et al.*,³⁶ Russo *et al.*³⁷ and Kock *et al.*³⁸ who observed that
26 elemental fractionation decreased when a fs laser pulse instead of a ns laser pulse was
27 used. The difference between the two lasers was attributed to the reduced thermal
28 alteration of the sample material. Therefore, shorter wavelength and shorter laser pulse
29 reduce elemental and isotopic fractionation. Little attention has been given to laser
30 interaction with biological matrices and references addressing effects of fractionation
31 in such matrices were not published. However, it is known that coupling of laser
32 radiation with the sample depends on the sample composition. For example, O'Connor
33 *et al.*³⁹ studied the effect of laser ablation when vanillic acid, pyrazinoic acid, nicotinic
34 acid and poly(vinyl alcohol) were added to sediment. In this study, they observed that
35 better analytical results were obtained when a laser radiation absorbing compound
36 (vanillic acid, pyrazinoic acid or nicotinic acid) was added to the sample. They also
37
38
39
40
41
42
43
44
45
46
47
48
49
50
51
52
53
54
55
56
57
58
59
60

1
2
3 found that discs prepared with vanillic acid had the highest optical absorbance at 213
4 nm, resulting in a lower ablation depth and better sensitivity, probably due to
5 formation of smaller particles during the ablation process.
6
7

8 Claverie *et al.*⁴⁰ investigated the aerosol produced by fs laser ablation of
9 polyacrylamide gels for Se detection in selenoproteins. Ablation of narrow lanes at
10 high repetition rate showed that up to 77% of particles were below 1 μm and the
11 transport efficiency of particles coming from the deepest ablation was lower. Laser
12 fluence was not found to influence the particle size distribution but permitted to
13 increase the amount of particles ablated. A 2-mm wide lane ablation was demonstrated
14 to be suitable for sampling as it permitted to bring sufficient amount of material
15 without affecting significantly the ICP ionization efficiency; neither significant plasma
16 temperature change nor matrix effect could be detected.
17
18
19
20
21
22

23 24 **Ablation cells**

25
26
27 In principle, the purpose of the ablation cell is to accommodate the sample. The cell
28 must isolate the sample from the ambient in order to hinder the entrance of air and to
29 avoid losses of ablated aerosol. Material is ablated from the sample and the formed
30 aerosol/particle is transported to the ICP by a flow of gas (carrier gas) where the
31 analyte is atomized and ionized. The carrier gas is passed through the cell at a constant
32 flow rate and the connection of the cell to the injector tube in the plasma torch is
33 usually through a polytetrafluoroethylene (PTFE) tubing (transfer line). PTFE tubing
34 of 100 cm length and 0.6 cm internal diameter are employed for this purpose. Different
35 ablation cells have been proposed, whose internal volume (in the range of 3 to 100
36 cm^3) and geometry are different. The ablation cell geometry and the transfer line play
37 an important role on the overall transport efficiency and signal profile. Investigations
38 have been made in order to improve transport efficiency, which is of the order of 10–
39 80% (see references 19, 41 and those cited therein). The volume of the ablation cell
40 affects mainly the dispersion of the signal and thus the magnitude of the
41 signal/background ratio. However, significant changes of aerosol transport efficiency
42 were not observed for ablation cells with different volume as well as for different
43 length of transfer lines.⁴² Cell design and simulations of aerosol behavior and its
44 transport were investigated,^{41,43-47} with the purpose of predicting the dispersion of the
45 aerosol and finding those parameters that affect its loss in the ablation cell. The
46 influence of the sample characteristic must also be considered and manufacturers of
47
48
49
50
51
52
53
54
55
56
57
58
59
60

1
2
3 LA systems in general provide cells to accommodate different sizes of samples. In the
4 case of soft biological tissues analysis, refrigerated ablation cell has been proposed.⁴⁷⁻⁴⁹
5
6 In this way, the sample can be analyzed directly, allowing its integrity and better
7 reproducibility, which is very important for obtaining bioimages.
8
9

10 11 **Analyte Measurement**

12 13 **Isotope Ratio**

14
15
16 Isotope ratio (IR) has been mostly investigated and applied in tracer experiments.⁵⁰⁻⁵¹
17
18 Instability of the ICP-source and laser ablation process as well as the limited precision
19 of quadrupole ICP-MS instruments (ICP-QMS) (0.2 to 1% of relative standard
20 deviation – RSD – for solution nebulization, which increases to 10 to 50% for laser
21 ablation), isobaric and polyatomic interferences, mass discrimination (bias), detector
22 dead time, memory effects, contamination, plasma instability, matrix effects, and
23 fractionation effects associated with LA are intrinsic limitations of IR measurements.⁵¹⁻
24
25 ⁵³ Fractionation effects can be reduced by using high laser power density (e.g. 10^9 W
26 cm^{-2}). Fractionation does not play a significant role for inter-element IR (e.g.
27 $^{67}\text{Zn}/^{64}\text{Zn}$) but does for intra-element IR (e.g. $^{206}\text{Pb}/^{238}\text{U}$) measurement. The mass
28 discrimination effect can be corrected using reference standards with certified IR
29 value. However, few isotopic standards are commercially available, which imposes
30 restriction for exact IR measurement in biological tissue samples.⁵⁴
31
32
33
34
35
36
37

38
39 Sector field (ICP-SFMS) or multicollector (ICP-MCMS) instruments have been
40 employed for more precise and accurate IR measurement (RSD of 0.01-1% can be
41 achieved) owing to their capacity to resolve polyatomic interferences, or to detect
42 isotopes simultaneously in the latter case. However, the high cost of these instruments
43 has clearly limited their applications in large scale. Additionally, more expertise is
44 necessary for operating these instruments as well as in working with stable isotope
45 tracer elements.⁵⁴ It is worth citing that LA-ICP-MS had been neglected in this area
46 and only one paper had been published until 2006.⁵⁵ Since then, several studies (see
47 Table 1) have been conducted and important information gained with respect to
48 population and living organisms habitat, migration, elements uptake by living
49 organisms and respective distribution, proteome, instrument performance, and
50 environmental pollution. A detailed discussion about stable isotope tracers used in
51 biological tissues analysis can be found elsewhere.⁵⁶
52
53
54
55
56
57
58
59
60

1
2
3 As can be seen in Table 1, precision, expressed by RSD, is usually worst for ICP-
4 QMS instruments. However, depending on the isotopes involved, reasonable results
5 can be obtained by employing ICP-QMS for IR measurement,⁵⁷ provided that mass
6 bias is rigorously corrected. Feldmann *et al.*⁵⁸ demonstrated the superior performance
7 of LA-ICP-MCMS in comparison to LA-ICP-QMS, for Zn IR measurement in tracer
8 experiments.⁵⁹ Errors were two orders of magnitude lower for LA-ICP-MCMS and less
9 number of samples were necessary to distinguish enriched samples over control ones.
10 Indeed, the high precision achieved with LA-ICP-MCMS rendered bioimages with
11 better resolution.
12

13
14 The bioavailability of Bi in implanting metals was accessed in a study conducted by
15 Urgast.⁶⁰ Images of thin tissue sections around the metal implant (as pellets) showed
16 that Sn, Pb and Bi apparently increased around the implant area as well as Zn, an
17 indication of inflammation process. However, too high RSD was observed for the
18 ²⁰⁸Pb/²⁰⁹Bi IR when measured using ICP-QMS, which could not determine migration
19 or not of Bi. Therefore, IR data are very important in biological material analysis but
20 ICP-MCMS instrument is recommended in order to obtain precise and accurate results.
21
22
23
24
25
26
27
28
29
30
31
32
33
34
35
36
37
38
39
40
41
42
43
44
45
46
47
48
49
50
51
52
53
54
55
56
57
58
59
60

Table 1 Applications and studies about IR in biological samples analysis using LA-ICP-MS

Sample	ICP-MS Instrument	Laser ablation Instrument/Wavelength	Measured IR	RSD (%)	Remarks	Ref.
Fish otoliths	ICP-SFMS Element 2	New Wave UP 213 UV/213 nm	$^{138}\text{Ba}/^{137}\text{Ba}$	1	Enriched ^{137}Ba (tracer) was transmitted from females to offsprings.	55
Fish otoliths (salmon)	ICP-SFMS Element 2 ICP-MCMS Neptune	CETAC LSX-213/213 nm	$^{135}\text{Ba}/^{138}\text{Ba}$ $^{137}\text{Ba}/^{138}\text{Ba}$	3-8	LA-ICP-MS allowed easy discrimination of specimens during all stages of fish life and information for metabolic Ba studies.	61
Fish otoliths (salmon)	ICP-MCMS Nu-Plasma	IR-fs-LA ALFAMET	$^{87}\text{Sr}/^{86}\text{Sr}$	0.02	Sr isotopic as signatures remained stable across years and could be used for habitat/migration salmon studies	62
Bone and tooth	ICP-SFMS Finnigan Element	Ablascope/213 nm	$^{87}\text{Sr}/^{86}\text{Sr}$	0.1-0.2	$^{87}\text{Sr}/^{86}\text{Sr}$ ratio was used as a migration indicator to identify ancient population mobility; wet plasma conditions were used; Rb separation allowed to good results	63
Daphia magna specimens	ICP-SFMS Element XR	New Wave Research (UP193HE ArF* excimer-based)/193 nm	$^{66}\text{Zn}/^{64}\text{Zn}$; $^{68}\text{Zn}/^{64}\text{Zn}$	~5	Ablation cell with lower internal volume to reduce wash-out effects; wet plasma conditions and medium mass resolution ($m/\Delta m \sim 2000$) were used; Zinc was preferably bio-accumulated in four areas (eye, gills, gastrointestinal tract and egg/embryo).	64
Gel spots containing bovine serum proteins separated by PAGE	ICP-QMS (Agilent 7500ce and Elan 6100)	LSX 100 and LSX 200 (CETAC)/266 nm	$^{65}\text{Cu}/^{63}\text{Cu}$; $^{65}\text{Cu}/^{34}\text{S}$ $^{64}\text{Zn}/^{65}\text{Cu}$	4-50	Zinc was rapid exchanged by ^{65}Cu in bovine serum albumin; MALDI-TOF was used to identify metal-binding peptides.	65
Rat frozen tissues	ICP-SFMS Element 2 and ICP-QMS Agilent 7700c	New Wave (NWR-213)/213 nm	$^{67}\text{Zn}/^{64}\text{Zn}$; $^{67}\text{Zn}/^{66}\text{Zn}$ $^{70}\text{Zn}/^{64}\text{Zn}$; $^{70}\text{Zn}/^{66}\text{Zn}$ $^{64}\text{Zn}/^{66}\text{Zn}$	14-80	Zinc (tracer) was enriched in muscle, liver and heart.	59
Oldest, newly formed and fully grown leaves of <i>Elsholtzia splendens</i>	ICP-QMS (Agilent 7500)	New Wave UP266 (266 nm)	$^{65}\text{Cu}/^{63}\text{Cu}$	10-15	The isotope ^{65}Cu (tracer) was accumulated in the petiole and the main veins of the leaves and the content of K, Mg, Mn, P and S was increased by the Cu-stress only for new leaves.	66
Pellets of powdered peat and lichen samples	ICP-MCMS (Isoprobe) or ICP-QMS (Thermo Elemental Plasma Quad3)	New Wave UP266 (266 nm)	$^{207}\text{Pb}/^{206}\text{Pb}$ $^{208}\text{Pb}/^{206}\text{Pb}$	0.3-1.1 (MC-ICP-MS) or < 14 (ICP-QMS)	LA-ICP-QMS could be used for Pb IR monitoring in such kind of samples; mass bias correction was necessary for improving precision on IRs measurements using ICP-QMS.	57
Pig liver and sheep liver sections	ICP-TOFMS (Renaissance, LECO)	CETAC LSX-200 (266 nm)	$^{63}\text{Cu}/^{65}\text{Cu}$; $^{64}\text{Zn}/^{66}\text{Zn}$	3-8	Cu was accumulated in different regions of sheep liver; optimized conditions for the LA (spot size and scan speed) and cryogenically cooled cell were used; ^{13}C was used as internal standard.	8

Table 1 – Continued

Rat brain tissues	ICP-MCMS (Neptune)	New Wave UP-213 (213 nm)	$^{67}\text{Zn}/^{64}\text{Zn}$; $^{67}\text{Zn}/^{66}\text{Zn}$ $^{70}\text{Zn}/^{64}\text{Zn}$; $^{70}\text{Zn}/^{66}\text{Zn}$ $^{64}\text{Zn}/^{66}\text{Zn}$	0.07-0.48	Zn tracers took longer time to arrive in hippocampus and amygdale than in cortex and hypothalamus	58
Gels spots separated by 1D or 2D PAGE of Alzheimer-diseased brain proteins samples or tau proteins doped with tracers	ICP-SFMS (Element) or ICP-QMS (Elan 6100)	Ablascope/213 nm or CETAC LSX 213 (213 nm)	$^{54}\text{Fe}/^{56}\text{Fe}$; $^{65}\text{Cu}/^{63}\text{Cu}$ $^{67}\text{Zn}/^{64}\text{Zn}$	10-15	The Cu IR indicated that Cu-containing proteins were stable upon the reducing conditions of GE; Zn IR demonstrated that some proteins can accumulate the isotopic-enriched tracer after GE; the Fe IR revealed that almost all proteins accumulated ^{54}Fe during the tracer experiments; $^{65}\text{Cu}/^{63}\text{Cu}$ and $^{67}\text{Zn}/^{64}\text{Zn}$ ratio in five different bands of gels revealed that tau proteins were able to bind Cu but not Zn after proteins separation using 1D GE; proteins were analyzed using MALDI-TOFMS.	67-69
Human urine (dried)	ICP-QMS (Elan 6000 or ICP-SF-MS (Element)	CETAC LSX200 (266 nm)	$^{235}\text{U}/^{238}\text{U}$ $^{230}\text{Th}/^{232}\text{Th}$	1-5	The $^{235}\text{U}/^{238}\text{U}$ ratio in urine could be applied in order to detect possible incorporation of exposed persons to depleted or enriched U.	70
Moss samples	ICP-SFMS (Element)	CETAC LSX200 (266 nm)	$^{236}\text{U}/^{238}\text{U}$ $^{234}\text{U}/^{238}\text{U}$ $^{240}\text{Pu}/^{239}\text{Pu}$	1.2-10	LA-ICP-MS can be utilized for IRs measurements of U and Pu radionuclides; LA-ICP-MS provides a very limited water load to the ICP-source, reducing uranium hydride formation ($^{238}\text{UH}^+ / ^{238}\text{U}^+$) and avoiding interference over ^{239}Pu but not Am.	71
Violet leaf, rose petal, and small piece of a gel (used in separation of human proteins by GE)	ICP-SFMS (Element)	Surelite II-10 (Nd:YAG), (532 nm)	$^{65}\text{Cu}/^{63}\text{Cu}$ $^{67}\text{Zn}/^{64}\text{Zn}$ $^{235}\text{U}/^{238}\text{U}$	3-15	Near field-LA-ICP-MS could be used to improve lateral resolution at nanometer scale range, which would be useful in cells and organelles studies.	72
Human Hair	ICP-MCMS (Neptune)	New Wave UP213 (213 nm)	$^{34}\text{S}/^{32}\text{S}$	< 0.05	Longitudinal isotope ratio variations in single hair strands could be used as an indicator of geographical origin and recent movements of individuals.	73
Limb of rats (where metal pellets were implanted)	ICP-QMS (Agilent 7500c)	New Wave UP213 (213 nm)	$^{208}\text{Pb}/^{209}\text{Bi}$	Too high (not informed)	Metals implants can increase Sn, Pb and Bi nearby the implant, but IR images were of low resolution and distinction was not possible by using ICP-ICP-QMS instrument.	60
Fish otoliths	ICP-MCMS (Nu Plasma HR)	CETAC LSX-200 (266 nm)	$^{87}\text{Sr}/^{86}\text{Sr}$	< 1%	Discrimination of life stage habits, hatchery and wild trout with 100% accuracy was achieved using multivariate analysis; the $^{87}\text{Sr}/^{86}\text{Sr}$ IR correlated positively with Sr concentration in water; the method could be used as isotopic fingerprint without tracer experiments.	74
Bivalve shell (exposed to enriched Ba and Mo isotopes)	ICP-QMS (Thermo XSeries 2; Perkin Elmer Elan DRC II)	Femtosecond LA (Alfamet, 1030 nm)	$^{97}\text{Mo}/^{95}\text{Mo}$ $^{135}\text{Ba}/^{137}\text{Ba}$	Not informed	Ba enrichment indicated direct incorporation of dissolved Ba into the shell in proportion to the levels in the water where they grew with a 6-8 day delay; neither the soft tissue nor the shell were significantly sensitive to Mo enrichment.	75
Fish scale	ICP-QMS (Elan 6000)	CETAC LSX200 (266 nm)	$^{88}\text{Sr}/^{44}\text{Ca}$	9.3	The migration pattern of fish (from sea or lake waters) was revealed by $^{88}\text{Sr}/^{44}\text{Ca}$ IR.	76

Table 1 – Continued

Fish Otoliths	ICP-MS (Nu Plasma HR)	NWR 193 excimer-based (193 nm)	$^{84}\text{Sr}/^{88}\text{Sr}$; $^{86}\text{Sr}/^{88}\text{Sr}$	<10	A method for the isotope pattern deconvolution (IPD) of an enriched Sr double spike used as a distinctive tracer in a biological system was developed, based on a transgenerational marking study of Sr isotope double spike (^{84}Sr and ^{86}Sr) from female spawners of carp (<i>Cyprinus carpio L.</i>) to the centre of the otoliths of their offspring.	77
ICP-MCMS: inductively coupled plasma-mass spectrometer with multicollector; ICP-SFMS: inductively coupled plasma-mass spectrometer with sector field						
ICP-QMS: inductively coupled plasma-mass spectrometer with quadrupole; (CRC) ICP-QMS: inductively coupled plasma-mass spectrometer with quadrupole and collision or reaction cell						
MALDI-TOF: matrix assisted laser desorption ionization - time of flight; GE: gel electrophoresis; IR: isotope ratio						

Calibration

Although LA-ICP-MS has progressed over the last two decades, allowing direct multi-element determination of major, minor and trace elements in a wide range of matrices (including biological tissues),⁷⁸⁻⁷⁹ different calibration strategies are usually required to obtain quantitative data. In fact, this is the main challenge for an extensive number of matrices because the standards available are limited. Matrix effects may be induced in the ablation process itself, during aerosol transport or in ionization process in the ICP.^{32,80-81} Thus, calibration must provide means to compensate or alleviate these differences among samples and standards in order to obtain quantitative data.

Quantification and calibration in the field of elemental imaging using LA-ICP-MS were reviewed by Hare *et al.*⁸⁵ Different strategies for element quantification in biological tissues using LA-ICP-MS have been employed.^{21,82-84} They involve internal standardization (IS), external calibration, standard addition, on-line standard addition, isotope dilution, matrix matched standards, and novel methods such as film coating and printing. Possibilities and limitations of element quantification using LA-ICP-MS are schematized in Fig. 1.

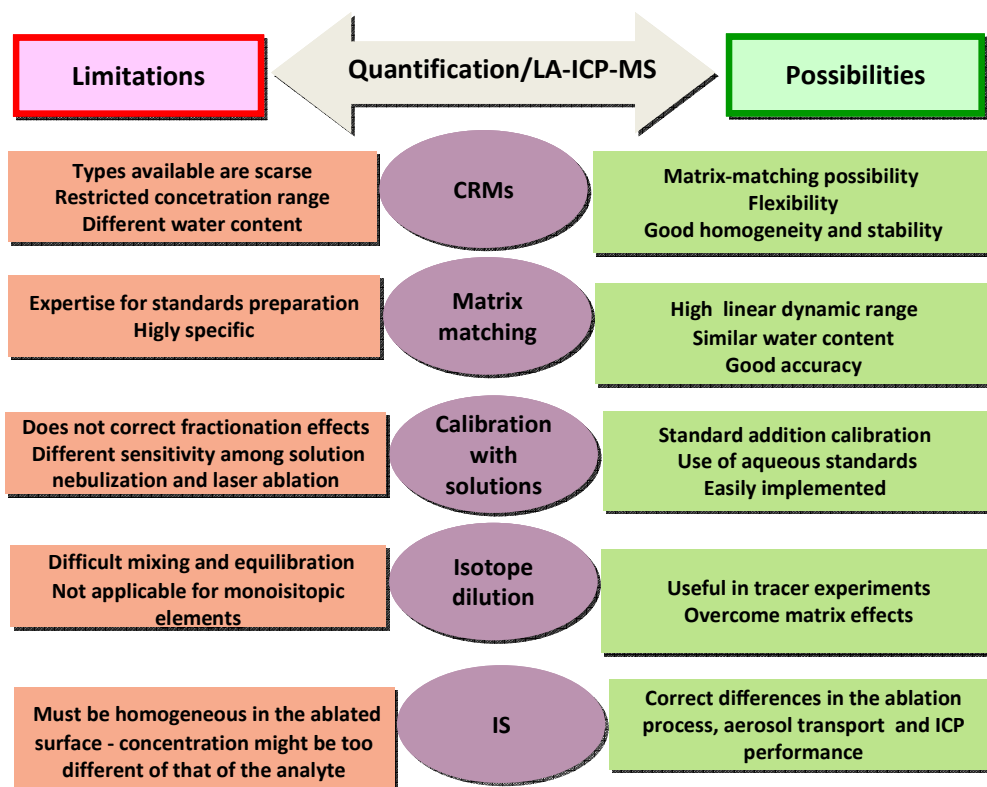


Fig. 1. Possibilities and limitations of element quantification using LA-ICP-MS. CRMs: certified reference materials; IS: internal standard.

Internal standardization

An internal standard (IS) can compensate fluctuations of laser power and fluency, differences in sample thickness, sample mass ablated and transported as well as instabilities and drifts taking place in the ion ICP-source. Differently of solution nebulization ICP-MS, the IS candidate for LA-ICP-MS must be usually naturally distributed within all sample. Criteria such as similar mass and ionization potential of the analyte should also be fulfilled, which imposes restrictions to proper IS selection. The IS and analyte should also suffer similar fractionation effects and similar interaction with the laser beam. Isotopes of C and S are potential IS candidates in biological matrices analysis using LA-ICP-MS. Although the ionization potentials of C and S are relatively high, isotopes of both elements are subject to spectral interferences, and may not be uniformly distributed within the biological tissue, reasonable results were obtained when C or S was used as IS. The choice of the IS isotope will depend on the type of instrument used, keeping in mind the interferences by polyatomic ions, which are more critical for ICP-QMS instruments.

1
2
3 The isotopes ^{43}Ca or ^{44}Ca were used to normalize the analyte signal in teeth layers⁸⁶⁻
4 ⁸⁸ and bone,⁸⁹⁻⁹¹ but it has been claimed that Ca varies significantly within the tooth.⁹²
5 Sulphur is a keratin matrix element and the isotopes ^{34}S and ^{32}S have been effectively
6 used as IS in the analysis of hair,⁹³⁻⁹⁴ ^{33}S in shell tortoise⁹⁵ and ^{32}S in nail⁹⁶. Sulphur is
7 bound to amino acids such as cysteine, methionine and cysteic acid and its
8 homogeneous distribution in such matrices is assumed. ^{13}C was used as IS in the
9 ablation of green leaves of oak trees.⁹⁷ Variations of C concentration between ribs and
10 other places of the leaf were not taken into account because the C content changed in
11 an acceptable range. Bei Wu *et al.*⁶⁶ and Dietrich *et al.*⁹⁸ used ^{13}C as IS in order to
12 compensate the water content effect and the possible inhomogeneity of the materials. A
13 linear relationship among water and ^{13}C signal was observed and the same was for ^{33}S
14 and ^{34}S , which reinforced that they could be used as IS to compensate the water effect.
15 The authors selected ^{13}C because its signal was higher than those of ^{33}S and ^{34}S . ^{13}C
16 was also successfully used as IS to cancel out variations in ablation, transport, and
17 ionization efficiency in sheep horn that is rich in keratin.⁹⁹ ^{13}C has also been used as IS
18 in other applications, including element quantification in rat brain tissue¹⁰⁰ and
19 urine.¹⁰¹

20
21 Conversely, other authors observed degradation of accuracy when ^{13}C was used as
22 IS.¹⁰²⁻¹⁰⁴ For an heterogeneous mixture of organic and inorganic materials (compost),
23 the accuracy of the results was worse than that obtained without normalization to ^{13}C .
24 ¹⁰² This was attributed to different C distribution within standards and samples (pellets
25 of soil spiked with aqueous standards were employed for calibration). However, the
26 authors stated that it was difficult to find another IS because its concentration must be
27 equal (or at least known) in samples and standards. Hoffmann *et al.*¹⁰⁴ suggested that
28 the signal intensity of ^{13}C should have the same magnitude of the analyte to avoid
29 concentration values tending to zero or infinity. However, this is in general
30 impracticable because the IS is naturally present in the biological solid sample. Todolí and
31 Mermet¹⁰⁵ cite that C may be present as a gaseous species or solid particles in the ICP.
32 This also applies to LA-ICP-MS, as C may be transported in the form of CO_2 , CO or
33 another gaseous/solid species, which differs remarkably of the analyte particles. Thus,
34 C can not completely compensate the effects above mentioned, affecting the accuracy
35 and precision of the results.

36
37 ^{232}Th and ^{238}U were used as IS for Cu, Fe, Zn, P and S imaging in human brain
38 tissue.^{69,103} Matrix matched standards spiked with the analyte and the IS elements were
39
40
41
42
43
44
45
46
47
48
49
50
51
52
53
54
55
56
57
58
59
60

1
2
3 prepared. Although ^{232}Th and ^{238}U have different ionization potential and mass of
4 those of the analyte, the authors stated they were feasible for the human brain imaging.
5 Austin *et al.*¹⁰⁶ compared the performance of raw analytical data and that normalized to
6 ^{13}C , ^{52}Cr , ^{53}Cr , ^{89}Y and ^{101}Ru for imaging experiments. These authors observed that
7 ^{13}C is a suitable IS candidate, which exhibited a linear response with respect to the
8 mass ablated, and apparent independence from the adjacent ^{14}N mass peak when the
9 ^{13}C signal in the sample was at least 6% of the raw signal. They also observed that ^{13}C
10 can compensate variations of sample drying, which occurs during long hours (~5 to 10
11 hours) of imaging experiments.
12
13
14
15
16
17
18

19 **Matrix-matched standards**

20
21
22 Becker *et al.*¹⁰⁷⁻¹⁰⁸ pioneered quantitative imaging by LA-ICP-MS in brain tissue,
23 using matrix-matched standards for calibration. Since then, a variety of matrix matched
24 standards were investigated and a great number of applications were carried out.^{2,109-120}
25 Standards prepared with certified reference materials (CRMs) can be used for matrix
26 matching calibration in LA-ICP-MS, but matrices available are quite limited. This
27 imposes severe restrictions, not only with respect to sample composition but also
28 elements with certified concentration. Hence, standards produced in-house have been
29 used for calibration.
30
31
32
33
34
35

36 In general, biological tissues whose matrices are similar to those of the samples are
37 spiked by known amounts of elements of interest.^{2,111-112,115-116,121-124} Procedures of
38 preparation of biological tissues standards are described by Becker *et al.*,¹⁷ Hare *et*
39 *al.*¹²⁵ and Lear *et al.*¹²⁶ The procedure for animal tissue consists in preparing a
40 homogenate of the tissue, followed by elemental spiking, frozen, cryocutting and
41 fixing on glass microscope slide.
42
43
44
45

46 Usually, the analyte concentration in the matrix matched standard prepared is
47 validated by digestion, prior determination using solution nebulization and ICP-MS,
48 whereas the homogeneity of the spiked elements within the standard is checked by LA-
49 ICP-MS. When CRMs are used, the different water content among CRMs and fresh or
50 frozen tissues (water content around 70-95%) is a concern. Depending on the case, the
51 CRM must be reconstituted with water.^{8,49,127}
52
53
54
55

56 Examples of matrix matching standards preparation and application are as follows.
57 Spiked whole blood or blood serum with known amounts of analyte were used by Pugh
58
59
60

1
2
3 *et al.*¹²⁸ for quantitative imaging of Sr, Gd and Pt in thin animal tissue sections. The
4 spiked blood or blood serum was placed in a customized frozen block of
5 carboxymethylcellulose, which was subsequently frozen and cryocut to sections with
6 20-60 μm thickness. Santos *et al.*¹²⁹ prepared standards of powdered mussel tissue,
7 dried snail and rat brain tissues for Cu, Zn, Cd, Hg and Pb imaging in marine snail.
8 The tissues were spiked with the analytes and pressed into discs. Calibration using the
9 snail tissue discs yielded better results owing to matrix similarity. Semi-quantitative
10 results were obtained using one-point calibration with mussel tissue. Wu *et al.*^{66,130}
11 prepared standards by spiking powdered certified apple leaves, followed by pressing to
12 obtain pellets, for imaging of K, Mg, Mn, Cu, P, S and B in leaves of plant. Standards
13 of cellulose powder⁹⁷ spiked with the analyte and pressed as pellet, or matrix matched
14 standards prepared from powder leaves spiked with the analyte and fixed on glass slide
15 were used for calibration and elements imaging in plant tissue.⁹⁸ Certified bone meal
16 (NIST 1486) was used to prepare standard in form of pellets for calibration and analyte
17 quantification in teeth and other calcified matrices as described by Hare *et al.*¹³¹
18 Stadlbauer *et al.*¹³² prepared standards of hydroxyapatite for quantification of elements
19 in bone and teeth. The hydroxyapatite was dissolved in HNO_3 , equilibrated with multi-
20 element standard solution, evaporated to dryness and then pressed into solid pellet. For
21 trace element quantification in mussel shells, Bellotto and Miekeley¹³³ prepared
22 calibration standards by coprecipitation of elements of interest into a CaCO_3 matrix,
23 which was then pressed into powder discs. Hair strands enriched with the
24 analyte⁹³⁻⁹⁴ or powdered laboratory hair standards placed on carbon tabs were
25 employed⁹³ for calibration and quantitative element determination in hair. Stable
26 standards of rat brain tissue (spiked with controlled amounts of elements of interest)
27 encapsulated in a sol-gel matrix produced by tetraethyl orthosilicate (TEOS) were
28 prepared by Sela *et al.*⁸⁴ for element imaging in animal tissue. Hare *et al.*¹⁰⁰ and Lear *et*
29 *al.*¹²⁶ prepared standards of homogenized chicken breast. The tissue was pressed into
30 moulds, spiked with elements of interest, frozen and cryocut to produce multi-point
31 calibration curves for element quantification in mouse brain. For Au and Ag
32 nanoparticles quantification in fibroblast cells, Drescher *et al.*¹³⁴ employed
33 nitrocellulose membrane for matrix matching calibration. A series of dried Au and Ag
34 nanoparticle droplets on nitrocellulose membrane were completely ablated and
35 analyzed by ICP-MS. Single fibroblast cells incubated with Ag or Au nanoparticles
36 were ablated and the number of particles per cell was estimated on the basis of these
37
38
39
40
41
42
43
44
45
46
47
48
49
50
51
52
53
54
55
56
57
58
59
60

1
2
3 calibration curves. According to Kumtabtim *et al.*,¹⁰¹ single droplets of urine spiked
4 with elements of interest and dried on a PTFE substrate were used for preparing
5 calibration curves for trace element quantification in Fabry disease patient urine.
6
7

8 9 **Solution based calibration**

10
11
12 Calibration with solutions has been investigated for quantitative analysis of biological
13 tissue using LA-ICP-MS. To this end, a nebulizer was adapted to the laser ablation
14 chamber, being the standard solution aerosol added inside the ablation chamber,¹³⁵ or
15 the aerosol from the ablation chamber and that from the nebulizer were mixed in the
16 ICP,¹³⁶⁻¹³⁷ or both aerosols were combined before introduction into the ICP by using a
17 bulb, Y, or T connector as mixing tool. The water introduced together with the dry
18 aerosol acts as buffer in the plasma,¹³⁸ improving plasma stability, accuracy¹³⁸ and
19 sensitivity.¹³⁶
20
21

22
23 Total consumption nebulizers or those that produce partially desolvated aerosol are
24 usually employed for calibration with solutions in LA-ICP-MS. With such nebulizers
25 the ablation chamber and transport line does not get wet, which would hinder the
26 analysis. In a study conducted by Günther *et al.*,¹³⁹ reduction of sensitivity was
27 observed for non desolvated aerosol; excessive water diluted the ablated aerosol and
28 also cooled the central channel of the ICP. Desolvation systems produce aerosol more
29 comparable to the LA-aerosol, reducing interferences (e.g. by oxides and hydroxides).
30
31

32
33 Calibration with aqueous standards was employed for quantitative elements imaging
34 in brain.¹³⁶ A dual flow consisting of the carrier gas (carrying the aerosol from the
35 ablation chamber) and the nebulizer gas (carrying the aerosol from a pneumatic
36 nebulization with aerosol desolvation) was used. Both aerosols were introduced
37 separately in the injector tube inside a special ICP torch and then mixed in the ICP.
38 Matrix matching was performed by solution nebulization of a series of aqueous
39 standards with defined analyte concentration with simultaneous laser ablation of brain
40 homogenate, followed by parallel nebulization of 2% (v/v) HNO₃ and laser ablation of
41 the brain sample. The ratio of the slope of calibration curve obtained by synthetic
42 laboratory standards prepared with mouse brain homogenate (spiked with elements of
43 interest at defined concentrations) and that obtained by using aqueous standards was
44 used to correct the difference of sensitivity among solution nebulization and laser
45 ablation. This approach was also used for element quantification in hair strands using
46
47
48
49
50
51
52
53
54
55
56
57
58
59
60

1
2
3 LA-ICP-MS. In this case, calibration curve obtained by ablating hair strands with
4 known analyte concentration was used for the sensitivity correction.¹³⁷ Karpas *et al.*⁹³
5 adapted the laser ablation chamber to an ultrasonic nebulizer with an aerosol
6 desolvator for U determination in powdered hair by LA-ICP-MS. Uranium standard
7 solutions were nebulized sequentially during the laser ablation of the powdered hair
8 samples fixed on carbon tabs. The concentration of U in hair was determined through
9 the calibration curve obtained by standard addition calibration.
10
11

12
13
14 A micronebulizer inserted directly into a cooled laser ablation chamber was applied
15 for solution-based calibration in brain tissue analysis for U and Th determination.¹⁰⁷
16 During laser ablation of thin sections of brain, defined standard solutions with
17 increasing analyte concentration were nebulized, whereby the calibration was
18 performed by a standard addition mode. For the correction of different element
19 sensitivities in nebulization-ICP-MS and LA-ICP-MS, a correction factor was obtained
20 by the ratio:concentration of element determined by solution-based calibration in LA-
21 ICP-MS/true concentration of element in the sample.
22
23
24
25
26
27
28

29 **Matrix-adapted standards**

30
31
32 Studies focusing the development of standards for LA-ICP-MS calibration are increasing.
33 Austin *et al.*¹⁴⁰ described the use of poly(methylmethacrylate) (PMMA) films containing an
34 organic solvent and organometallic standard spin coated over quartz slide. The accuracy and
35 precision obtained in the determination of Cu and Zn (using Y and Ru as IS) through
36 calibration with the PMMA standards were comparable to those obtained for conventional
37 matrix-matching ones. The results indicated a suitable degree of matrix-matching provided by
38 the PMMA film. Thin films of agarose gels were evaluated by Stärk *et al.*¹⁴¹ Aqueous
39 solutions of agarose spiked with defined amounts of the analytes were cast and subsequently
40 dried, producing films with average thickness of 3 μm in the centre. However, the analytes
41 were not homogeneously distributed across the whole film. Then, a defined region of the film
42 was selected for analytical purposes. Analysis of cell cultures was carried out by LA-ICP-
43 MS, using the agarose films to obtain calibration curves. The results obtained were in
44 accordance with those previously found by nebulization ICP-MS. Bellis and Santamaria-
45 Fernandez¹⁴² employed ink jet patterns as model for elemental mapping, with reference to
46 biological samples. An ink jet printer with copper-containing cyan ink to create lines and 2D
47 patterns was used. Copper concentration was controlled by varying the colour density
48
49
50
51
52
53
54
55
56
57
58
59
60

(transparency) of the image whilst features from 100 μm to $> 1 \text{ mm}$ were employed. Precision improved with increasing feature size and Cu concentration. The ablation chamber was interfaced with solution nebulization, whereas Ge was used as IS. The authors state that this approach can provide an accurate 2D visual representation of element distribution within samples. The colour density showed a linear relationship with Cu concentration. The method developed showed spatial resolution of at least 100 μm . Hoesl *et al.*¹⁴³ developed internal standardization and calibration procedures for elemental imaging in biological samples like Western blot membranes and tissue sections. The procedures are based on printing spiked inks onto the top of thin layer samples for simultaneous internal standardization and calibration of LA-ICP-MS. One ink contains the IS whereas the other ink contains lanthanides for calibration, allowing the quantification of metal tagged proteins after electro-blotting in Western blot immunoassays. The inks spiked with lanthanides were printed with different densities on nitrocellulose membranes in well-defined squares to produce matrix-matched standards. The lanthanides tagged proteins and antibodies on nitrocellulose membranes as well as the prepared standards were quantified by LA-ICP-MS. The LOD was typically lower than 4 fmol and RSD of 1-2% was observed. Konz *et al.*¹⁴⁴ described Au sputtering over the sample surface to produce film and use ¹⁹⁷Au as IS instead of ¹³C for imaging of Mg, Fe and Cu in histological tissue of eye. Considering the type of sample analyzed, the authors stated that Au sputtering is a more reliable, precise and robust methodology than traditional internal standardization with ¹³C. Cheajesadagul *et al.*¹⁴⁵ introduced doped keratin film standard for Pb quantification along hair strands. Lead doped keratin film standards were prepared by precipitation of hair protein solution casting in Pb standard solutions in the presence of trichloroacetic acid as a denaturant. The method was applied to quantitatively determine Pb distribution along a single human hair strand.

Isotope dilution

Isotope dilution (ID) can provide quantitative and accurate results. The sample is spiked with a known amount of an enriched isotope followed by appropriate mixing and equilibration. Ideally, the amount of spike must be such that the new isotope ratio is 1 to 10. The new isotope ratio of the involved isotopes is measured and the analyte concentration in the sample is quantitatively calculated. For this purpose, two stable isotopes of the element free from isobaric/polyatomic interferences are required. In the case of direct solid sample analysis, particles size and homogeneous incorporation of the spike within the sample matrix are mandatory. The latter requirement has surely

1
2
3 limited the implementation of ID as a quantification method for imaging experiments
4 using LA-ICP-MS. On-line addition or uniform spike deposition on the sample surface
5 seems satisfactory and preferable over conventional mixing. However, the guarantee of
6 complete and truly homogeneous distribution/incorporation of the spike within the
7 sample cannot be ensured.
8
9

10
11 The ID applicability for solid samples analysis by LA-ICP-MS was experimentally
12 demonstrated by Tibi and Heumann¹⁴⁶ - seven certified reference materials (aquatic
13 plant, skimmed milk powder, river sediment, wheat flour, bovine liver and estuarine
14 sediment) with a range of matrix constituents (organic and inorganic) were evaluated.
15 Solid pellets of the powdered samples were prepared by adding known amount of
16 enriched isotopes of Cr, Fe, Cu, Zn, Sr, Cd and Pb. To calculate the analytes
17 concentrations, the $^{52}\text{Cr}/^{53}\text{Cr}$, $^{56}\text{Fe}/^{57}\text{Fe}$, $^{63}\text{Cu}/^{65}\text{Cu}$, $^{67}\text{Zn}/^{68}\text{Zn}$, $^{86}\text{Sr}/^{88}\text{Sr}$, $^{111}\text{Cd}/^{113}\text{Cd}$,
18 and $^{206}\text{Pb}/^{208}\text{Pb}$ ratios were measured by means of ICP-SFMS. Although
19 contamination, spike equilibration time and particle size fractions demanded extra
20 investigations to ensure accuracy, the authors stated that ID can be applied for reliable
21 element quantification in powdered sample analysis using LA-ICP-MS.
22
23

24
25 Another strategy was used by Boulyga *et al.*,⁷¹ for ^{239}Pu , ^{240}Pu and ^{241}Am
26 determination in moss, which is a bioindicator to assess the occurrence of airborne
27 pollutants. Enriched ^{242}Pu and ^{243}Am were spiked in moss samples, followed by
28 ashing, leaching, and Pu and Am separation by ion chromatography. Droplets of the
29 separated Pu or Am chromatography fraction were placed on a stainless steel target by
30 electroplating and then analyzed using LA-ICP-MS. Good agreement between LA-
31 ICP-SFMS and alpha spectrometry results were observed for Pu isotopes, but not for
32 ^{241}Am . The authors stated that, in general, ID and LA-ICP-SFMS allows Pu isotope
33 ratio measurement with good accuracy and precision, avoiding possible errors
34 associated with losses during sample preparation. However, plasma instability,
35 inhomogeneous analyte distribution on the target sample and instability of the laser
36 ablation rate affected the precision and accuracy. Thus, application of LA-ICP-MCMS
37 was proposed to improve precision.
38
39

40
41 A methodology was developed by Becker *et al.*⁷⁰ for determination of U and Th in
42 urine, which was spiked with enriched U and Th ($^{235}\text{U}/^{238}\text{U} = 17.34$ and $^{230}\text{Th}/^{232}\text{Th} =$
43 3.64). After homogenization in ultrasonic bath, aliquots of the homogeneous urine
44 were dried and analyzed by LA-ICP-SFMS. The precision (between 1 and 5%) was
45 slightly better for U than for Th. The U and Th concentrations found in urine using
46
47
48
49
50

1
2
3 external calibration and ID were in satisfactory agreement. Sela *et al.*⁹³ determined U
4 in powdered hair using on-line isotope dilution. A solution of an enriched isotope
5 (²³⁵U) was nebulized through an ultrasonic nebulizer adapted to the ablation chamber.
6
7 The hair sample was ablated (to evaluate the results) and an additional ablation of the
8 hair sample together with nebulization of the spike solution was carried out. The
9 change in isotope ratio was used to calculate the U concentration. A ICP-SFMS
10 instrument was employed.
11
12
13

14 Isotope dilution has been applied for metals binding proteins identification, where
15 metals bound to proteins separated by gel electrophoresis (GE) can be directly
16 determined by LA-ICP-MS. The area of interest in the gel is more precisely analyzed
17 using LA-ICP-MS instead of digesting the gel spots with protein assignments prior to
18 metal detection using solution nebulization and ICP-MS. Electrophoresis combined
19 with LA-ICP-MS for the identification and quantitation of metal binding proteins was
20 firstly described by Neilsen *et al.*¹⁴⁷ Human serum enriched with Co was subjected to
21 electrophoresis and the agarose gels corresponding to the first (1D) and second (2D)
22 dimensions were interrogated and analysed using LA-ICP-MS. Comparison of the
23 distribution map for Co with the protein distribution map obtained via Coomassie
24 Brilliant Blue staining allowed identification of main Co binding serum proteins. The
25 element was shown to be principally associated with albumin, α_2 -macroglobin, β_1 -
26 lipoprotein, α_1 -lipoprotein, α_1 -antitrypsin and haptoglobin. Sussulini and Becker¹⁴⁸
27 reviewed the combination of polyacrylamide gel electrophoresis (PAGE) and LA-ICP-
28 MS for metallomic studies, highlighting advantages and limitations of this
29 combination.
30
31
32
33
34
35
36
37
38
39
40

41 Konz *et al.*¹⁴⁹ used species-specific isotopic dilution (SSID) as an absolute
42 quantification strategy to determine Fe-bound transferrin (Tf) in human serum
43 separated by non-denaturing GE. The ratio ⁵⁶Fe/⁵⁷Fe was measured using ICP-SFMS,
44 whereas the spike was an isotopically enriched ⁵⁷Fe-Tf complex. The authors stressed
45 that the ablation procedure (single line ablation over perpendicular direction to the
46 electrophoretic migration) and the sample preparation (nonstained gels and
47 nondenaturing PAGE) need careful attention to ensure adequate precision and
48 accuracy. The quantification revealed accurate and precise results not only by
49 analyzing the protein spot in the middle position but also in the adjacent ablation line
50 to the center. Compared with other quantification methodologies, the sample analysis
51 time was reduced to less than 15 minutes. Deitrich *et al.*¹⁵⁰ utilized SSID for absolute
52
53
54
55
56
57
58
59
60

1
2
3 quantification of Cu and Zn in gel spots containing superoxide dismutase (SOD)
4 enzymes of bovine liver, separated using GE. The intrinsic metals of the metalloprotein
5 were used for labelling of the isotopically labelled spike (^{65}Cu -SOD, ^{68}Zn -SOD). In
6 this study, ^{13}C was used as IS. No interferences or cross contamination from
7 neighbouring lanes distorted the LA-ICP-MS measurement and no isotopically
8 enriched Cu and Zn originally bound to SOD was liberated and transferred to other
9 binding proteins. This work demonstrated the potential of ID combined with GE and
10 LA-ICP-MS for quantitative SOD determination as also cited by Bettmer¹⁵¹ in a
11 comprehensive review article. Kutscher *et al.*¹⁵² developed a method for determination
12 of ovalbumin labeled with p-hydroxy-mercuribenzoic acid (pHMB). Polyacrylamide
13 GE was used for protein separation followed by Hg quantification using ICP-MS. Two
14 different quantification strategies were applied: external calibration using
15 standards of the derivatized protein after ^{13}C normalization and, as a proof of
16 concept, SSID using pHMB spiked with ^{199}Hg . Due to the inhomogeneous distribution
17 of the protein within the gel bands, it could be demonstrated that the ID approach was
18 superior in terms of precision and accuracy. Using SSID, the measured isotope ratio
19 ($^{202}\text{Hg}/^{199}\text{Hg}$) in the gel corresponded to recoveries between 95% and 103%. Yang *et*
20 *al.*¹¹¹ determined selenomethionine (SeMet) in yeast using SSID and ICP-MS. The
21 isotope ^{74}Se was enriched in the SeMet spike. The method was based on the off-line
22 spotting of high performance liquid chromatography (HPLC) fractions onto a
23 polystyrene substrate followed by laser ablation and introduction of the dried micro-
24 droplet residues into the ICP for Se determination. Concentrations were obtained based
25 on measured $^{78}\text{Se}/^{74}\text{Se}$ and $^{82}\text{Se}/^{74}\text{Se}$ ratios (RSDs < 1% for n = 4) and were in good
26 agreement with those obtained using direct HPLC-ICP-MS. The authors affirmed the
27 proposed method is a satisfactory alternative for quantification of SeMet in yeast. An
28 absolute quantification of intact proteins was reported by Esteban-Fernandez *et al.*,¹⁵³
29 where metal coded affinity tags (MeCATs) combined with GE separation, ICP-MS
30 detection and SSID were used. Albumin or transferrin in human serum were determined
31 in the GE spots by using LA-ICP-MS. The MeCAT(Yb)-IA labeled proteins was
32 spiked with a known amount of standard proteins labeled with isotopically enriched
33 MeCAT(^{171}Yb)-IA in a proportion 1:2 and then separated. Three parallel lanes for each
34 protein were measured around the spot maximum. The isotope ratio $^{172}\text{Yb}/^{171}\text{Yb}$ was
35 used in ID calculations. Spot mineralization and laser ablation led to similar
36 concentration values, but direct laser ablation of the gel resulted in fast determination,
37
38
39
40
41
42
43
44
45
46
47
48
49
50
51
52
53
54
55
56
57
58
59
60

making the quantification of proteins in biological samples in only one working day feasible.

A workflow of the associated application of GE, ID, LA-ICP-MS for protein separation, element quantification, and protein detection by MALDI/ESI-MS (matrix assisted laser desorption ionization-mass spectrometry/electrospray ionization-mass spectrometry)¹⁵⁴ is schematized in Fig. 2.

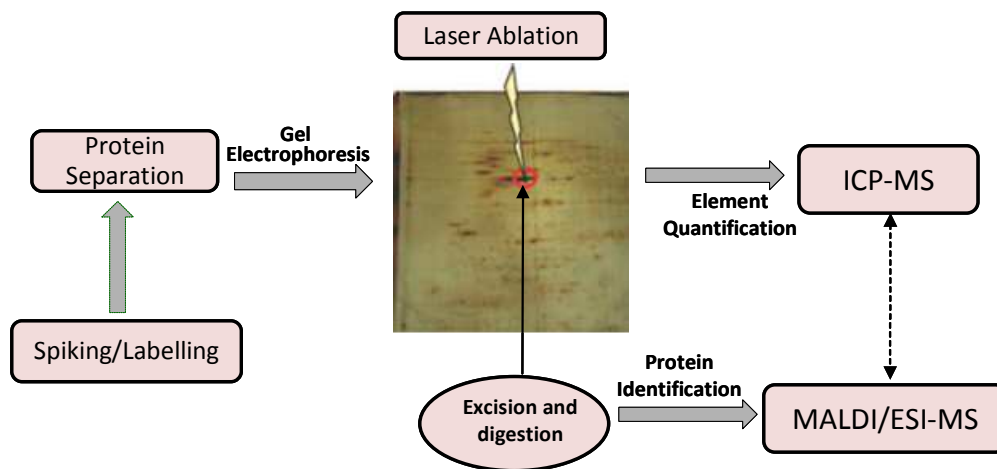


Fig. 2. Combination of ID, GE, LA-ICP-MS and MALDI/ESI-MS in proteome studies.

Bioimaging

Since 1994, when elemental imaging (or mapping) of thin tissue sections by means of LA-ICP-MS was firstly described by Wang *et al.*,⁷ more than one hundred articles have been published in the area, mostly from 2011, and it is believed the number of publications will grow in forthcoming years.

Laser ablation-inductively coupled plasma mass spectrometry has been extensively employed to produce images of element distributions in human and animal (brain, liver, bone, teeth, cells etc.) and plant tissues. In several dedicated papers and reviews, techniques such as X-ray fluorescence microscopy (XFM), particle induced X-ray emission (PIXE), energy dispersive X-ray spectroscopy (EDS), scanning micro-X-ray fluorescence spectrometry (μ -XRF), and secondary ion mass spectrometry (SIMS) were compared with LA-ICP-MS for imaging of metals and metalloids in biological tissues.^{9,13,15-16,155-159} When compared to the other techniques, the main advantage of LA-ICP-MS is higher sensitivity, or lower matrix

1
2
3 effect or simplicity. Imaging by LA-ICP-MS has been reviewed by the Becker *et al.*^{9-10,154,160-}
4
5 ¹⁶¹ An overview of the latest achievements in LA-ICP-MS methods and applications for
6
7 bioimaging is presented in their most recent review.¹⁷

8 In general, the information gained with imaging of major components as well as trace
9
10 elements in animal tissue samples can help to understand biological processes and clarify
11
12 questions in biomedical research. Using LA-ICP-MS, Hare *et al.*¹⁶² created a three-
13
14 dimensional atlas of Fe, Cu and Zn by aligning quantified images of the metals distribution in
15
16 sections of cerebrum and brainstem of mouse. This atlas can facilitate the study of these
17
18 metals in the brain and help to elucidate their role in neurobiology. Applications of LA-ICP-
19
20 MS for imaging of animal tissues as well as metalloproteins in gels after electrophoresis
21
22 separation are cited in Table 2.

23 **Sample preparation and image generation**

24
25
26 Either paraffin-embedded or native frozen (stored at temperatures about -70 °C) sections are
27
28 in general employed to fix animal tissue on glass microscope slide for further LA-ICP-MS
29
30 analysis. The tissues samples are sliced to about 20-200 µm thickness and deposited on the
31
32 slide. Imaging of native cryo-sections (20 - 30 µm thick) was introduced by Becker.¹⁷ Plant
33
34 tissues or leaves can be directly fixed on glass slide with double-sided tape¹⁶³ for LA-ICP-MS
35
36 measurements or cut into sections and fixed in glass slide by means of resin.¹⁶⁴ Teeth and
37
38 bone⁹¹ can be mounted in epoxy resin. Fixed and cryoprotected tissue of murine brain was
39
40 critically investigated by Hare *et al.*¹⁵⁵ They investigated losses of elements and sample
41
42 contamination and observed that 99.78% of K and 78.01% of Mg were leached from brain
43
44 tissue during fixation and cryoprotection. Losses of water soluble elements like Fe, Cu and Zn
45
46 ranged from 26.61 – 31.62%. Ca and Sr either retained or absorbed metal ions from the
47
48 sucrose solution used in sample treatment. They concluded that metal leaching is highly metal
49
50 specific and that preparatory steps for cryosectioning of brain tissue should be approached
51
52 according to this specificity.

53
54
55 Three-dimensional images can be created by repeatedly scanning a specimen. As the
56
57 ablated region is roughly the same depth at each point, multiple images can be created and
58
59 stacked to form the image. Both the thickness of the tissue and the laser parameters should be
60
61 optimised for each specific application. For the analysis of dried tissues, the laser ablation
62
63 process can be performed at room temperature. However, the application of cooled laser
64
65 ablation cells (commercially available from selected laser ablation companies or developed

in-house) has proved to be advantageous, not only for the analysis of cryopreserved materials, but also for dried biological samples.^{48,107}

For element imaging in soft tissue laser ablation is destructive to the specimen, where pit size is below 200 μm deep. Quantification using this technique usually requires laboratory matrix-matched standards. Matrix-matched standards and sample for imaging by LA-ICP-MS analysis must be analyzed under identical experimental conditions. For quantification, average ion-responses of individual raster are plotted against calibration curves, whereas the analyte is usually normalized to that of an IS as discussed before. To obtain images of element distribution, the tissue section is ablated line by line, covering the entire section area. Appropriate laser scan speeds may be calculated by considering the relationship between laser scan speed, laser spot diameter and the total scan cycle.¹⁶⁵ Images of elements distribution are obtained using the MATLAB software¹¹¹ or other written in house.^{114,166-168}

The time dependent ion intensity raw data obtained from the mass spectrometer is usually transformed into spreadsheet format using the Excel software for further data analysis. In general, the software for imaging takes into account parameters such as line length, number of lines, data offset at start and at end, as well as the diameter of the laser beam and the distance between the lines. The pixel size of the resulting images is dependent of line distance, number of spots and spot diameter. Pixel dimensions for biological tissue imaging has been reviewed by Becker *et al.*¹⁷ A workflow of bioimaging of rat brain tissue section using LA-ICP-MS and element quantification is schematized in Fig. 3.

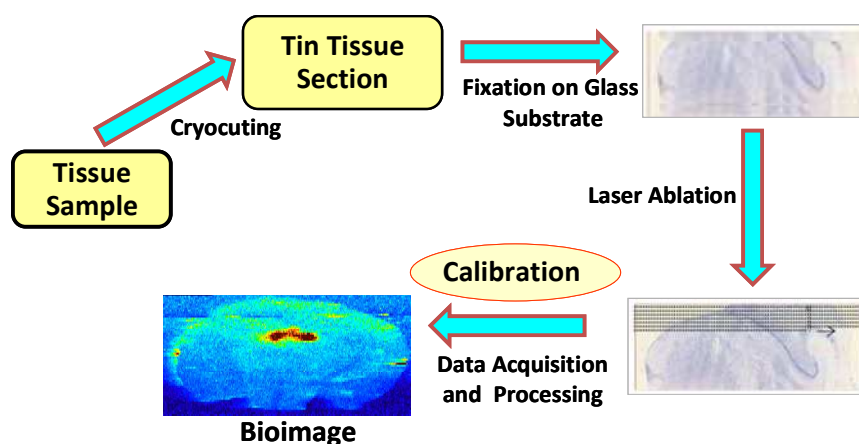


Fig. 3. Workflow for quantitative element bioimage in rat brain tissue using LA-ICP-MS, from sample preparation to image generation.

1
2
3 Improved spatial resolution can be achieved through use of narrow beam diameter and
4 low laser rastering rate, but at the expense of time and sensitivity. Control of section thickness
5 is also a critical experimental variable thus requiring laser energies sufficient to achieve
6 complete ablation at specified section thicknesses. The measurement time for imaging of
7 biological tissues (up to several hours) also depends on the size of the tissue area analyzed.
8
9

10
11 Images of trace elements distribution in tissue sections by LA-ICP-MS is typically
12 performed using spatial resolutions of 30-50 μm and above. A higher resolution image is
13 desirable for many biological applications. The limiting factor for increasing resolution is the
14 sensitivity of the ICP-MS technique, where signal-to-noise ratio is poor due to inherent
15 background spectral interferences and reduced sample volume introduced into the ICP with
16 decreasing laser beam diameter. "Dry" plasma conditions in LA-ICP-MS gives rise to lower
17 polyatomic interferences in comparison to "wet" plasma, as the production of polyatomic
18 interferences from water is lower. However, interferences are still present for a number of
19 biologically relevant isotopes that will eventually result in element responses that do not
20 exceed the background signal. The major sources of the interferences are from major elements
21 in the sample and impurities from the atmosphere, carrier gas and plasma gas, namely CO_2 ,
22 N_2 , H_2O and O_2 .¹²⁶ These interferences can be reduced or eliminated by employing
23 quadrupole instruments equipped with dynamic or collision reaction cells^{126,169-170}, ICP-
24 SFMS, and ICP-MCMS instruments^{112,122}.
25
26
27
28
29
30
31
32
33
34
35
36
37
38
39
40
41
42
43
44
45
46
47
48
49
50
51
52
53
54
55
56
57
58
59
60

Table 2 Elements imaging of animal tissues using LA-ICP- MS

Element	Sample	Remarks	Ref.
Sr, Gd, Pt, Zn	Rat tumour tissue (Gd); whole rat - sections (Sr); rat brain (Pt)	Quantitative image of metallo drugs (Sr, Pt based) and MRI contrast agent (Gd based) was obtained; Pt was distributed in the left brain hemisphere and was restricted to this region with minor exception of some transport across the corpus callosum; it was suggested that some areas of the tumor had become necrotic resulting in build-up of Gd in occluded vasculature; Sr was elevated in hard tissue.	128
C, P, Fe and Zn	Rat brain slices: formaline fixed brains with induced strokes by photothrombosis (PT) and by transient Main Cerebral Arterial Occlusion (tMCAO), and from a fresh brain obtained from a healthy rat	Clustering based on multi-element distribution using a simple k-means algorithm was able to segment the tissue in anatomically meaningful regions; the distribution of some elements in fixed tissue was qualitatively different from that in fresh tissue; the accumulation of elements in the rim of the lesion produced by PT showed a unique pattern that was not replicated in the tMCAO model of stroke; in fixed tMCAO as well as in fresh tissue the distribution of elements in the white and grey matter showed characteristic patterns.	171
Cu, Mn, Fe and Zn	Parkinsonism mouse model brains	Elevated concentrations of Cu, Mn, Fe and Zn within the <i>substantia nigra</i> (SN) are suspected to play a role on the development of Parkinson's disease; Fe concentration within the SN of the lesioned animals increased significantly when compared against control animals.	100
Li, Mn, Fe, Cu, Zn, Rb	Sections of mouse brain	It was possible to distinguish the element concentrations in different brain regions.	136
Fe, Cu, Zn, and Mn	Native brain sections of mice subchronically intoxicated with 1-methyl-4-phenyl-1,2,3,6-tetrahydropyridin (MPTP) as a model of Parkinson's disease	Significant decrease of Cu concentration in the periventricular zone and the <i>fascia dentata</i> at 2 h and 7 days of intoxication and Cu recovery or overcompensation at 28 days were observed; in the cortex Cu decreased slightly whereas Fe increased in the interpeduncular nucleus but not in the SN, indicating role of Cu availability in Parkinson's disease.	109
P, S, Fe, Cu, Zn and C	Sections of rat brain samples	Images of P, S, Fe Cu and Zn concentrations were obtained; P, S and Fe distribution revealed the depletion of these elements in tumor tissue; the shape of the tumor could be clearly distinguished from the surrounding healthy tissue by the depletion in C.	112
Fe, Gd, Pt	Rat brain under convection enhanced delivery of Gd nanocomplex into brain and convectional enhanced delivery; pig brain with co-infusion of Gd contrast agent and carboplatin (chemotherapy drug) into brain	Image obtained <i>via</i> LA-ICP-MS complimented magnetic resonance image (MRI), revealing distribution of contrast agent and nano-particle based drug formulation; regions of hyperintensity in MRI caused by Gd were consistent with ^{57}Gd images derived by LA-ICP-MS; mapping of Fe enabled assignment of anomalous contrast enhanced regions in control rat brain that, if LA-ICP-MS had not been used, could have been incorrectly attributed to Gd rather than to haemorrhage; the quantitative results for Pt confirmed that the concentrations of carboplatin in tissue was sufficient to kill glioblastoma cells.	172
^{56}Fe , ^{57}Fe	Mouse brain	Enhanced sensitivity with the reaction cell allowed construction of high resolution ($6\ \mu\text{m}^2$) quantitative imaging of ^{56}Fe and ^{57}Fe in the mouse brain that approached the dimensions of single cells.	126
Cu, Zn, Pb, U	Thin tissue sections of primary human brain tumors (glioblastoma multiforme - GBM) and adjacent non-neoplastic brain tissue	Tumor mass region and tumor invasion zones, respectively, were clearly detected by LA-ICP-MS measurements; quantitative images of the spatial distribution of Cu, Zn, Pb and U were compared with conventional histology and receptor autoradiographic methods, which allowed the precise localization of the elements in the tumor and the tumor invasion zone.	111

Table 2 - Continued

As species	Human skin	The penetration and accumulation of As is strongly dependent on its speciation; arsenosugars penetrated through the unbroken skin at a similar rate as arsenate; arsenite and DMA(V) were taken up percutaneously at a rate which was more than a factor of 29 and 59 higher than that of arsenate; accumulation of arsenosugars and DMA(V) was minimal, whereas arsenate and arsenite accumulated in the epidermis and in the dermis; no significant species transformations were observed.	173
P, S, Cu, Zn, C	Rat brain tissues (including tumor regions); rat kidney	Carbon, Cu and Zn distribution in a rat brain tissue containing a tumor was clearly seen by partly a deficit of Zn and C; Cu showed heterogeneous distribution within the tumor corresponding to areas of different degrees of vitality and necrosis at an overall higher level compared to the healthy contralateral hemisphere; a small tumor was detected in rat brain tissue by Cu/Zn, Cu/C or Zn/C ratios, characterized by a significant depletion of $^{63}\text{Cu}/^{64}\text{Zn}$ ratio.	174
Nd	Rat brain sections	Imaging of distribution in rat brain tissue stained in Nd solution revealed fine structures in brain.	175
Fe, Cu, Zn, Mn, and Ti, Na, K, Mg, Ca, C, P, S	Native cryosections of mouse heart	Metal and nonmetal images (quantitative for Zn, Cu, Ti, Mn and Fe) showed clearly the shape and the anatomy of the heart tissue investigated; all elements were inhomogeneously distributed.	114
Mn, Fe, Cu, and Zn	Sections of mouse liver tissue	Quantitative results showed that the average concentrations of Mn in control and Wilson's disease liver samples were not different; Fe, Cu, and Zn in Wilson's disease liver samples were found significantly higher than in control tissue samples; the average concentration of Cu was 30 times increased in liver of rat with Wilson's disease experimentally induced.	166
Cu, Zn, Cd, Hg, Pb, C, S	Longitudinal tissue sections of marine snail (<i>Nassarius reticulatus</i>)	The imaging (quantitative for Cu, Zn, Cd, Hg and Pb, and qualitative for C and S) revealed an inhomogeneous distribution for all elements investigated: S and C were distributed uniformly across the snail's body; Cu and Zn were distributed most broadly and were also found in the reproductive tract, in parts of the testis (male) and oviduct (female) but not in the ovary; Cd and Hg accumulation was restricted to the digestive gland, whereas lower level of Pb was also found in the testis and ovary; Cu, Cd and Pb were detected in kidney; all elements seemed to accumulate mainly in the digestive gland.	129
Au/Ag tagged antibodies bound to tissue	Archival formalin-fixed paraffin-embedded (FFPE) sections of normal gastric mucosa, normal breast and breast cancer; tissue microarrays (TMAs), taken from FFPE tissue blocks	The distribution of two breast cancer-associated proteins, MUC-1 and HER2, was evaluated; measurement of HER2 levels were well below the working range for a microscopic evaluation; comparisons with optical microscopy indicated the high sensitivity of the LA-ICP-MS technique; measurement of the immuno Au/Ag probes yielded impressive sensitivity for the target antigens (MUC-1 and HER2) and with enhancement factors of 70–130 for Ag relative to Au as a result of the metallation reaction.	176
Tb, Tm, Ho	Breast cancer tissue (primary antibodies labeled with lanthanides)	Simultaneous detection of three different breast cancer markers (HER2, CK 7, and MUC-1) was accomplished in a single tissue section under optimized LA-ICP-MS conditions; the direct comparability is of great benefit for standardization of the results in immunohistochemistry (IHC).	177

Table 2 - Continued			
Ca, P, S and Zn	Sections of 10 and 20 μm thickness of the fresh water crustacean <i>Daphnia magna</i>	LA-ICP-MS was compared with micro-XRF (X-ray fluorescence) and LA-ICP-MS was particularly sensitive for determining Zn in <i>Daphnia magna</i> , while the detection power of micro-XRF was insufficient; LA-ICP-MS was inadequate for the measurement of S distribution, which could be better visualized with micro-XRF due to interference by O_2^+ species in ICP-MS.	178
Eu, Ho, Tb, Tm, Lu, Pr	Cytochromes (CYP) P450 in liver microsomes of untreated and inducer treated rats	Lanthanide labeled antibodies were electrophoretically separated and CYP proteins blotted were identified and quantified; CYP1A1, CYP2B1, CYP2C11, CYP2E1 and CYP3A1 were simultaneously quantified; microsomes of rats treated with 3-methylcholanthrene, phenobarbital and dexamethasone showed increased levels of CYP1A1, CYP2B1 and CYP3A1, respectively.	179
Ce and I	Microsomes enriched in cytochrome - CYP1A1 and CYP2E1 - of rat liver and minipig duodenum; specific monoclonal antibodies directed against enzymes differentially labelled with Eu via a covalently linked chelator and with I, respectively	Both Eu and I were coupled to the heavy and the light chains of the antibodies; CYP1A1 and CYP2E1 enzymes were concomitantly detected; duodenal microsomes of minipigs orally exposed to polycyclic aromatic hydrocarbons showed a clear CYP1A1 signal; low levels of CYP2E1 could also be detected; LA-ICP-MS exhibited sensitivity similar to that of conventional chemoluminescence detection via peroxidase-labelled secondary antibodies.	180
Zn	Section of slug (Genus Arion)	Images of quantitative distribution of total Zn in a section of a slug sample and Zn-containing proteins after one-dimensional separation by gel electrophoresis (Blue Native PAGE) were obtained; no Zn was detected in the 1D gel lane of the belly skin, whereas three sharp peaks corresponding to Zn-containing proteins were found for the digestive gland; no Zn-proteins were detected in the foot skin.	181
Al, Br, C, Pt	Appendix, lymph nodes, fallopian tube and esophageal tumor tissues	Elemental imaging was used to elucidate the distribution of histological stains haematoxylin and eosin; the optical distribution of the stains was in very good accordance with the generated elemental images; Pt containing unstained and stained samples revealed that the staining procedure did not affect the distribution and the maximum signal intensity of Pt in esophageal tissue.	170
Cu, Zn, Pb and U	Tissue sections of primary human brain tumors (glioblastoma multiforme - GBM) and adjacent non neoplastic; rat brain tissues with tumor cells implanted	After implantation of tumor cells in one hemisphere of the rat brain and following 18 days of tumor growth, the tumor region with depletion and local enrichment of Cu was clearly detected; images of Cu, Zn, Pb and U were quantitative.	122
Mg, Fe and Cu	Tissue sections of fixed eyes iris, ciliary body, cornea and trabecular meshwork), embedded in paraffin, from human donors (cadavers)	Internal normalization with $^{197}\text{Au}^+$ sputtered on the sample surface allowed simultaneous qualitative determination of element distribution in tissue structures having different compositions and morphology, improving imaging of Mg, Fe and Cu in ocular tissue sections.	144
Cu and Zn	Neighboring sections of human brain tissue.	Distribution profiles of Cu and Zn in the adjacent sections of human brain tissue were quantified; inhomogeneous distributions of C, Cu and Zn were found and they were similar for all neighboring sections.	116
Ca, Cu, P, Mg, Sr, Zn	Calcium phosphate based crystals in knee cartilage and synovial fluid from arthritic patients, or hip arthroplasty	Distribution patterns of elements such as Cu and S did not correlate with the crystal deposits; crystal-associated elements, including Ca, P and Mg, were considered consistent with the presence of crystal deposits, observed in osteoarthritis knee cartilage and synovial fluid samples.	169

Table 2 – Continued			
Pt	Kidney mouse treated with cisplatin; human lymph node sections	Images for the staining agents (eosin and haematoxylin) as well as for the chemotherapy drug cisplatin in thin tissue sections were obtained; Pt was heterogeneously distributed in the kidney with an accumulation in the cortex.	182
Cd, Se, Cu, Te	Mouse lung	Control and QD (quantum dot)-inhaled samples revealed distribution of Cd atoms in the lungs arising from QDs accumulated in the bronchiolar area; the spatial distributions of ¹¹⁴ Cd and ⁸² Se suggested that the QDs underwent no obvious degradation in the lung tissue during a span of 17 days; the LA-ICP-MS data compared with hematoxylin and eosin stained images revealed that the inhaled QDs appeared in the same locations as the lymphocytes accumulated in the lungs.	183
Pt	Intraperitoneal tumor in healthy rat or receiving Pt-containing chemotherapeutic drug oxaliplatin and perfusate solution	Quantitative images of ¹⁹⁵ Pt distribution in the tumor sections revealed that changes in drug treatment, with temperature or additional administration of drug, did not drastically altered drug concentration or the extent of drug penetration in the tumor.	184
C, P, S, Ni, Cu, Fe, Gd, Zn	Mouse leg tumor (induced) where Gd-doped iron oxide nanoparticles (Gd-IONPs) were injected	Distribution of Gd correlated with that of Fe; C, P, S, and Zn distribution revealed that the effect of magnetic fluid hyperthermia (MFH) treatment was dependent on the diffusion of the magnetic fluid in the tissue; enrichment of Cu after MFH treatment was observed, probably due to inflammation in the tumor; abnormal distribution of Ni suggested a probable biochemical reaction in the tumor.	185
Au, Ag	Single fibroblast cells incubated with Ag or Au nanoparticles	Nanoparticles were visualized with respect to cellular substructures and were found to accumulate in the perinuclear region with increasing incubation time of the cells.	134
P, Mn, Zn, Fe and Ca	Colony of Escherichia coli 24 h-old	Colonies grown on nylon membranes over agar were ablated, yielding three-dimensional elemental maps, whereas a convex morphology consistent with visual inspection was observed; by normalizing the analyte signal to Mg elemental heterogeneity within the colony was observed; Mn content in the perimeter was higher than in the colony interior, whereas the converse was true for Ca.	186
⁶⁴ Zn, ⁶⁷ Zn, ⁶⁷ Zn, ⁷⁰ Zn	Liver, muscle, heart of rat treated with ⁶⁷ Zn and ⁷⁰ Zn tracers	Images revealed the incorporation of Zn stable isotopes in thin section of tissue; about 3-fold fraction of Zn was exchangeable within 1-2 days in the liver and a 2-fold fraction in aorta wall compared to muscle tissue; the largest change in isotope ratios was found for the animals that had been injected with a high dose of Zn 24 h before termination.	59
Zn, Cu, Fe, Pb, Mn, Ag	Rat kidney tissue	Protein complexes, extracted with water, were separated in their native state in the first and second dimension (2D) by blue native gel electrophoresis (BN-PAGE); bioimaging of metals in specific spots in the 2D gels were obtained as well as metalloproteins detection.	187
Mn, Fe, Cu, Zn, and Cd	Human liver (healthy and fibrotic/cirrhotic livers)	Most metals were homogeneously distributed within the normal tissue, whereas they were redirected within fibrotic livers resulting in significant metal deposits; Fe and Cu concentrations in diseased liver were found about 3-5 times higher than in normal liver samples.	188
Mn, Fe Cu Zn, Rb, P and C, S.	Mouse spinal cord	Quantitative element images of the spinal cord revealed its architecture; the “butterfly” shape of the central spinal grey matter was visualized in positive contrast by the distributions of Fe, Mn, Cu and Zn and in negative contrast by C and P; Mg, Na, K, S and Rb showed a more homogenous distribution; Zn but not Cu was enriched in the central channel.	189

Table 2 – Continued

1				
2				
3				
4				
5				
6				
7	Ti, V, Al,	Nanosilver-coated bone implant	Metal distribution within cancellous bone could be visualized for Ag as well as for nanosilver-coated bone implant constituents (Ti, V, and Al); Ag, Ti, and Zr displacement from the implant surface into the surrounding tissue was visualized; Ag was detected at a distance up to 750 μm from the implant surface, with only small amounts of Ag remaining.	190
8	Zr, Ag			
9				
10				
11	Zn, Sr, Cd	Deciduous incisors tooth of children	Quantitative images revealed that Pb, Zn and Cd were higher in dentine particularly in regions adjacent the pulp; the heterogeneity of the elements throughout the tooth structure that corresponded to specific structural and developmental features of teeth was displayed; clear demarcation of element deposition in regions of tooth associated with developmental periods was observed.	131
12	and Pb			
13				
14				
15				
16	Ba, Sr, Zn,	Root tooth of fossilized brown bear (<i>Ursus arctos</i>)	The cementum and dentine on a slice of the sample surface were clearly distinguishable, especially changes in elemental distribution in the summer and winter bands in the fossil root dentine; migration and diet of the bear were determined on the basis of variations in Sr/Zn ratio and their contents; there was an increase in the Sr/Zn ratio during the winter season caused by a reduction of food intake during hibernation; the measured Sr/Ca and Sr/Ba profiles across the sample showed seasonal fluctuations and proved the migration of this bear between his hibernaculum location and the place where the fossil was found.	191
17	Ca and P			
18				
19				
20				
21				
22	U, Th	Early Pleistocene equid tooth	The tooth showed a concentration gradient from the top to the base, indicating the U profile had not equilibrated after >1 Ma; the spatial pattern of $^{230}\text{Th}/^{234}\text{U}$ and $^{234}\text{U}/^{238}\text{U}$ indicated complex U-mobilization processes over the last 100 ka, dominated by small-scale redistribution of U; leaching from the tooth through the pulp cavity started at least 93 ka ago with several later phases in various domains of the dentine and cement.	192
23				
24				
25				
26	Na, Mg, K,	Articular cartilage	The quantitative LA-ICP-MS imaging of Gd confirmed the observation that the spatial distribution of Gd from [Gd(DTPA)] ₂ -contrast agent in the near-equilibrium state is highly inhomogeneous across cartilage thickness with the highest concentration measured in superficial cartilage and a strong decrease toward the subchondral bone; Na, Cl and K were detected with a higher accumulation in superficial cartilage layers compared with deep cartilage layers, whereas Mg, P, Ca, Ti and Zn increased from cartilage surface toward calcified region and subchondral bone.	193
27	Ca, Ti, Zn,			
28	C, P, S, Cl,			
29	P			
30				
31				
32				
33	Mn	Osteoblasts in calvarial organ cultures	Imaging of Mn (paramagnetic) showed that DIV4 (4 days in vitro) specimens sequestered more Mn than DIV25 (25 days in vitro) specimens and that reduced levels with preferential uptake of Mn by the posterior regions of the superficial zone occurred on day 25; the Ca and P elemental maps confirmed that the levels of both elements at the calvarial surface was higher for DIV25 compared with DIV4, possibly due to the maturation of mineralized deposits.	194
34				
35				
36				
37	Mg, Zn, P,	Teeth	Images of reactionary dentine (Rd) in response to polymicrobial invasion in teeth, including the distribution of the major mineral components, revealed a marked redistribution of Ca and P in Rd together with an increase of diffusely deposited Mg compatible with the mineral deposition phase of synthesis of the altered matrix; the abundance and distribution of elements (Mg, Zn, P and C) involved in biomineralisation were altered in carious teeth compared to healthy teeth.	195
38	C, Ca			
39				
40				
41				
42				
43				
44				
45				
46				
47				
48				
49				

Table 2 – Continued

Pb	Human primary teeth	Lead in dentine adjacent to the dentinoenamel junction may reflect the variation in Pb uptake during the pre- and neonatal periods; the spatial distribution of Pb in the dentine reflected the blood-lead levels.	196
----	---------------------	--	-----

Plant Tissues

Elemental distribution in plant tissues using LA-ICP-MS provides information such as potential of metal-accumulator plants¹⁶⁴ for remediation and amelioration of contaminated soils, elements uptake by plants¹⁹⁷ and further translocation/accumulation^{98,163,198-201} and respective effects^{66,202-203}. An example of elemental distribution for Se and S in sunflower (*Helianthus Annuus* L.) leaves is given in Fig. 4.

In Figure 4A it is observed that Se is present mainly at the tip of the leaf corresponding to plants treated with Se after 29 days of cultivation. When the Se distribution is compared with the image obtained for S distribution (Fig. 4B), a correlation between both elements is noted (Se promoted the translocation of S to the leaves and also activated the S uptake pathway). Probably, Se can replace S in amino acids, indicating that the metabolism of S can change in the presence of high concentration of Se. The leaf after 45 days of cultivation reveals that the levels of Se increased *ca.* 5-fold when compared with the leaf studied after 29 days, as can be seen in Fig. 4C. In this case, the distribution of Se is quite homogeneous in all regions of the leaf. N Fig. 4D is shown that the S level increased when compared with the leaf after 29 days of cultivation, being mainly concentrated at the tip of the leaf. By comparing Se treated plants and the control group (Fig. 4E and 4F) it is observed that both Se and S levels are lower in the control plants.

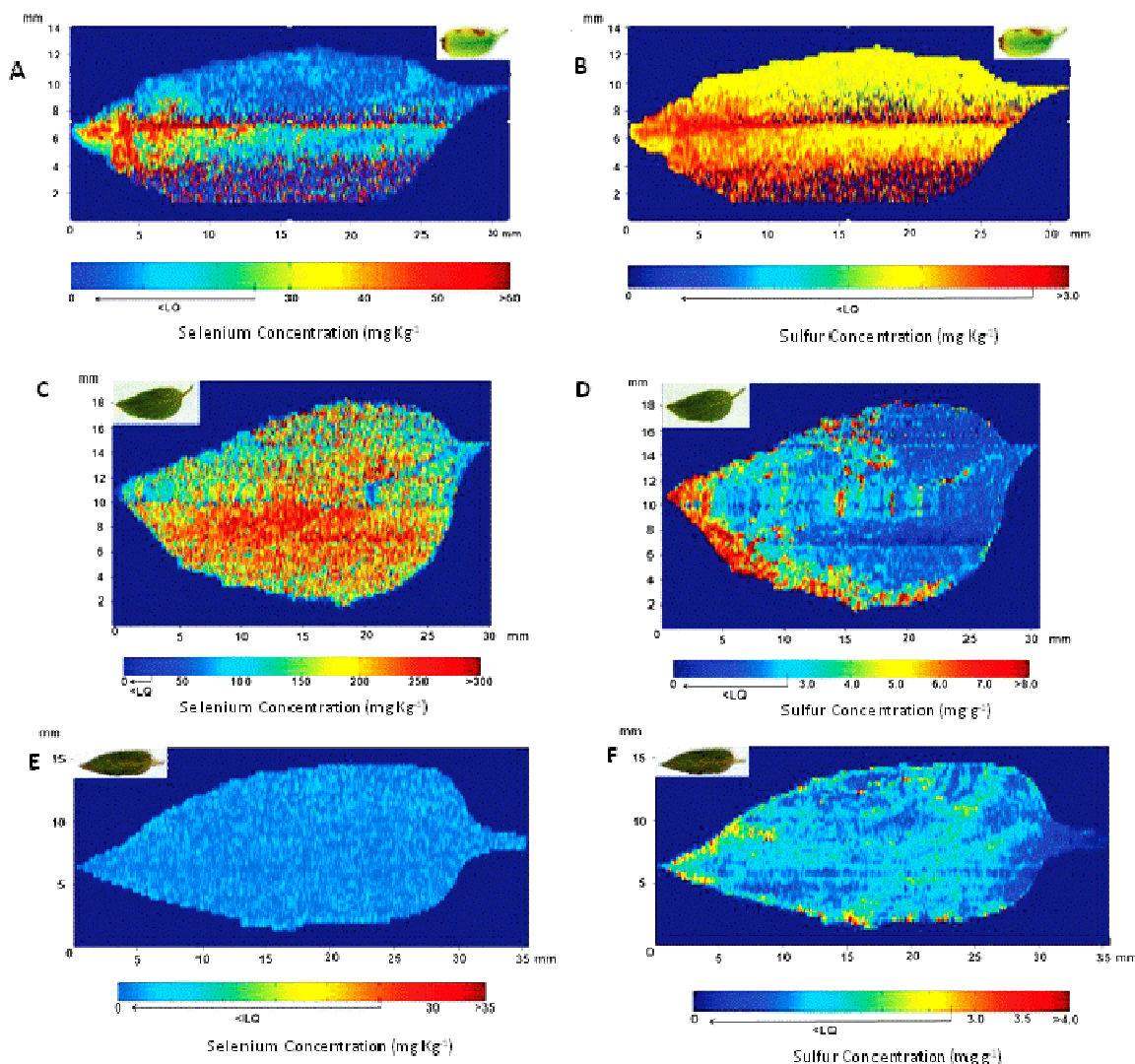


Fig. 4. Se (images A, C and E) and S (images B, D and F) distributions observed in sunflower leaves after 29 (A and B), 45 (C and D) and 50 (E and F) days of cultivation. Plants of leaves A and B were irrigated with 106 mg of Se, and in C and D with 174 mg of Se. Both Se and S distributions are shown in the sunflower leaves (E and F) collected from the control group after 50 days of cultivation. The picture of each leaf analyzed is shown on the upper left side of the image. *Reprinted from reference 203.*

Other studies and applications of LA-ICP-MS were conducted and important information was thus obtained as follows. Elements distribution in a cross section of maize root revealed that Hg ions does not cross the endodermal barrier of maize plants and, therefore, Hg is not uptake by the maize plant.¹⁹⁷ Accumulation of Mg, P and K at the boundary zone between the wounded and healthy tissue of sitka spruce (*Picea sitchensis*) bark suggested major role of Mg, P and K in non-specific response to wounding.⁶⁶ In root cross-sections of a Ni-hyperaccumulator plant (*Berkheya coddii* Rossler) higher Ni concentration was observed in

1
2
3 the cortex than in the stele, while the opposite was found for control root plants not exposed
4 to elevated Ni levels, suggesting that an active uptake or ion selection mechanism exists for
5 the plant in the absence of available Ni in the rhizosphere.¹⁶⁴ Au bioimage in rice (*Oryza*
6 *sativa L.*) shoots exposed to Au nanoparticles (AuNPs) revealed AuNPs distribution in
7 mesophyll and vascular areas, depending on organ or AuNPs concentration. Anionically
8 functionalized AuNPs showed higher translocation to rice shoots than did AuNPs and cationic
9 derivatives.²⁰⁴ Lead accumulated preferably in the vein structure of cayenne pepper
10 (*Capsicum annuum L.*)¹⁶³ while Mn and K accumulation were not affected by Pb.²⁰¹ Copper
11 accumulation and the effect of Cu stress on essential element uptake in newly formed leaves
12 of *Elsholtzia splendens* were observed, while no significant changes were found in the fully
13 grown leaves due to short-term Cu tracer treatment, showing the path of Cu uptake via the
14 petiole and main veins of the leaves.⁶⁶ Elemental distribution images of a developing wheat
15 grain showed that considerable amounts of nutrients were stored in the scutellum of the
16 embryo, which might be related to the high gene expression of element transporters in the
17 scutellum. Root primordia and leaf primordia were enriched in Mn and Zn, respectively.²⁰⁵
18 For potato grown in impacted mining region, LA-ICP-MS analysis showed that the
19 concentration of As in the skin was on average approximately 75 times greater than that of the
20 potato flesh; As was deposited between 200 and 1000 μm from the outer surface of the potato,
21 demonstrating that most of the As is present within the skin and not on its outer surface.²⁰⁶
22 Imaging of the distribution of dissolved P around *Brassica napus* revealed localized P release
23 along root axes and at root apices and differential P uptake efficiencies among two
24 investigated *B. napus* cultivars.²⁰⁷ Bioimages of rhizome cross-sections of hay-scented fern
25 growing on contaminated soils demonstrated that Pb and Sb were concentrated in the
26 periphery of the rhizome. In highly contaminated sites Pb was highest in the outer starchy
27 cortex bordering the vascular tract, contrary to control rhizomes, suggesting a secondary
28 accumulation mechanism that occurs after a certain threshold of Pb accumulation in the
29 rhizome. The Pb versus Sb concentrations in both rhizome and frond organs were highly
30 correlated suggesting similar biochemical and environmental factors influencing Pb and Sb
31 bioavailability and transport to above ground organs. It was evidenced that one reason for the
32 phytotoxicity of Pb is the displacement of nutrient metals.²⁰⁸
33
34
35
36
37
38
39
40
41
42
43
44
45
46
47
48
49
50
51
52
53
54
55
56
57
58
59
60

Hair

The pioneering work of Rodushkin and Axelsson²⁰⁹ described the use of LA-ICP-MS for quantitative determination of 71 elements along hair strand. The spatial resolution achieved with LA-ICP-MS translated into time allows images of elements distribution to intervals shorter than a day along a hair strand. The length profiles of detected elements are usually plotted starting from the hair root to the tip where quite different distribution pattern of elements are observed along the hair strands analysed. The distribution of Pt in a hair strand of a women treated with cisplatin is shown in Fig. 5.

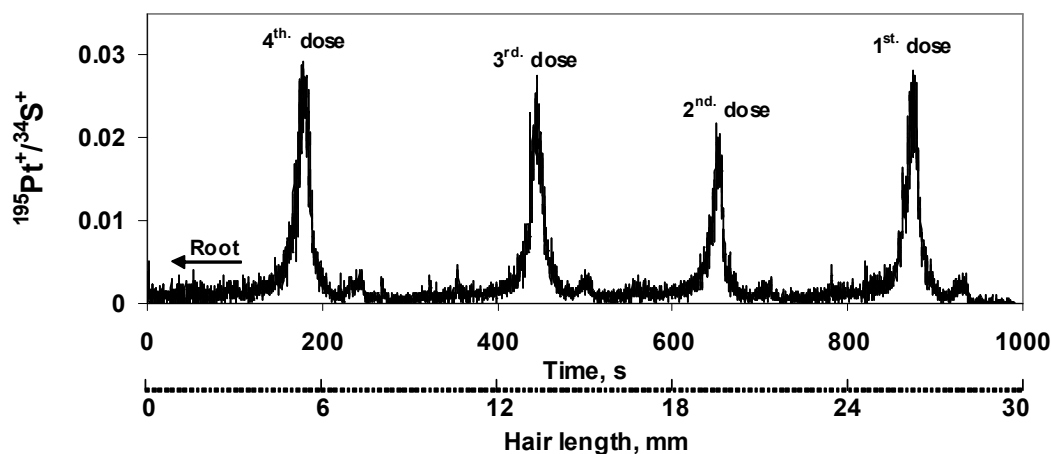


Fig. 5. Ratio of $^{195}\text{Pt}^+ / ^{34}\text{S}^+$ along a hair strand from a patient treated with four 100-mg doses of cisplatin. Reproduced from reference 94.

The potential of LA-ICP-MS to detect Hg in single human hair with a resolution corresponding to less than one day of growth was demonstrated.²¹⁰ Such high resolution analysis is not practical with most other techniques as the resolution is set by physically cutting the hair into segments and separately processing and analyzing each individual piece. Thus, the ability of LA-ICP-MS for rapid acquisition and tracking elemental concentrations or isotope ratio variation⁷³ along hair strands may be useful for prediction of geographical origin,⁷³ movements of individuals^{73,93,211} or provide information on diet and lifestyle⁷³ as well as exposition history to nutrient or toxic elements.^{93,137,145,211-215} Mercury concentration in the hair of a deceased person allowed to determine the time he was poisoned by Hg.²¹⁶ Variation of Pt concentration in hair strands was useful to monitor cisplatin metabolism by a patient treated with the drug (Fig. 5), preventing excessive administration of the drug.⁹⁴

1
2
3 Uranium concentration observed along a hair strand correlated with changes in the level of U
4 in drinking water.⁹³ Mercury variations along the entire length of individual grizzly bear hair
5 demonstrated a relationship between Hg accumulation rate in the hair and Hg intake through
6 the fish diet.²¹⁷ It was found that that 70% of the coastal grizzly bears sampled had Hg levels
7 exceeding the neurochemical effect level proposed for polar bears, providing valuable
8 information on the exposure to Hg.
9
10
11
12

13 14 **Conclusions and perspectives** 15

16
17 The LA-ICP-MS technique has been primarily applied for years in the geological field due
18 to features such as easy surface analysis, precise isotope measurements and multi-elemental
19 capability. However, the extensive list of references in this review demonstrates that this
20 technique has received a significant attention over the last 10 years and has been widely used
21 for analysis of biological samples. In fact, although its widespread applicability upon the
22 biological area, calibration strategies still act as a major weakness for LA-ICP-MS, hindering
23 its establishment as primarily choice for rapid, sensitive and accurate quantitative technique.
24 Some concluding remarks about the use of LA-ICP-MS in the biological field are as follow.
25
26
27
28
29

30 (i) Although a significant progress has been made in quantitative LA-ICP-MS
31 analysis with respect to calibration and signal normalization approaches, hesitation still exist
32 to accept as quantitative the analytical results generated by this technique. This implies on the
33 reliability of the spatial profiles (imaging) obtained and accuracy of determinations made by
34 using LA-ICP-MS.
35
36
37

38 (ii) Development of standards for biological matrices analysis using LA-ICP-MS is
39 necessary, as well as fundamental studies about fractionation and/or matrix effects with
40 respect to such matrices.
41
42
43

44 (iii) Even using ID and fs-laser, systematic tests to search the best approach for signal
45 treatment (i.e. normalization by using appropriate IS or mimicking by matrix-matched
46 standards) is a precondition to compensate matrix-induced interferences taking place on the
47 laser beam/sample surface interaction, dry aerosol transport and particles ionization in the
48 ICP.
49
50
51

52 (iv) Appropriate validation of bioimages obtained using LA-ICP-MS are required.
53 However, this is an analytical challenge due to lack of sensitivity, semi-quantitative capability
54 or needing of synchrotron radiation of the other techniques used for imaging. For that reason,
55 independent methods based on bulk elemental content have been applied to validate the
56 results obtained using LA-ICP-MS. However, this approach does not truly validate spatial
57
58
59
60

1
2
3 elemental profile point-by-point; micro-local sampling techniques such as laser micro-
4 dissection²¹⁸ could fulfill this task.

5
6 (v) Dedicated software commercially available are required for easier handling the
7 huge amount of data collected along the scanning, saving time and improving information
8 extraction for images generation. In addition, the long time required for high-quality spatial
9 elemental imaging calls for more robust/stable ICP-MS instruments to avoid signal
10 fluctuations arising from plasma flicker or instrument drift. Complete particle atomization and
11 ionization in the ICP as well as higher ion transmission from ICP through detector and truly
12 simultaneous isotope detection are topics to be considered.

13
14 (vi) Combination of LA-ICP-MS with molecular mass spectrometry techniques such
15 as MALDI-MS, ESI-MS or IM-MS (ion mobility) allows spatial distribution of elements and
16 protein structures identification, which has provided useful insights on biomolecular and
17 medical research.

18
19 (vii) Experiments with stable isotope tracer and IR measurements by LA-ICP-MS
20 represent a breakthrough topic in the field of metabolism and trace elements kinetics research
21 at a molecular level. Research in this area usually require an on-demand cooperation of
22 researchers with different expertise in the field of analytical chemistry, biology, nutrition,
23 medical and environmental areas, working in a multi-disciplinary scenario to achieve
24 comprehensive conclusions.

25
26 (viii) Laser ablation instruments with higher spatial resolution would allow analysis
27 of cells and cells organelles scale range, making possible studies of biochemistry processes in
28 real time.

29
30 (ix) The combination of simultaneous elemental and molecular mass spectrometry
31 imaging approach based on LA sampling, introduced for spatially resolved speciation
32 analysis, results in low LOD and high spatial resolution. This combination offers new
33 possibilities to address complex challenges in life science research.¹⁸²

34 35 36 37 38 39 40 41 42 43 44 45 46 47 48 **References**

- 49
50
51 1. B. Fernandez, F. Claverie, C. Pecheyran and O. F. X. Donard, *TrAC-Trends Anal.*
52 *Chem.*, 2007, **26**, 951-966.
53 2. J. Dobrowolska, M. Dehnhardt, A. Matusch, M. Zoriy, N. Palomero-Gallagher, P.
54 Koscielniak, K. Zilles and J. S. Becker, *Talanta*, 2008, **74**, 717-723.
55 3. A. L. Gray, *Analyst*, 1985, **110**, 551-556.
56 4. B. J. Fryer, S. E. Jackson and H. P. Longerich, *Can. Mineral.*, 1995, **33**, 303-312.
57 5. N. I. Ward, S. F. Durrant and A. L. Gray, *J. Anal. At. Spectrom.*, 1992, **7**, 1139-1146.
58
59
60

- 1
 - 2
 - 3
 - 4
 - 5
 - 6
 - 7
 - 8
 - 9
 - 10
 - 11
 - 12
 - 13
 - 14
 - 15
 - 16
 - 17
 - 18
 - 19
 - 20
 - 21
 - 22
 - 23
 - 24
 - 25
 - 26
 - 27
 - 28
 - 29
 - 30
 - 31
 - 32
 - 33
 - 34
 - 35
 - 36
 - 37
 - 38
 - 39
 - 40
 - 41
 - 42
 - 43
 - 44
 - 45
 - 46
 - 47
 - 48
 - 49
 - 50
 - 51
 - 52
 - 53
 - 54
 - 55
 - 56
 - 57
 - 58
 - 59
 - 60
6. S. F. Durrant and N. I. Ward, *J. Anal. At. Spectrom.*, 2005, **20**, 821-829.
7. S. Wang, R. Brown and D. J. Gray, *Appl. Spectrosc.*, 1994, **48**, 1321-1325.
8. A. Kindness, C. N. Sekaran and J. Feldmann, *Clin. Chem.*, 2003, **49**, 1916-1923.
9. J. S. Becker, M. Zoriy, A. Matusch, B. Wu, D. Salber, C. Palm and J. S. Becker, *Mass Spectrom. Rev.*, 2010, **29**, 156-175.
10. J. S. Becker, *Int. J. Mass Spectrom.*, 2010, **289**, 65-75.
11. R. Lobinski, C. Moulin and R. Ortega, *Biochimie*, 2006, **88**, 1591-1604.
12. J. S. Becker, A. Matusch, J. S. Becker, B. Wu, C. Palm, A. J. Becker and D. Salber, *Int. J. Mass Spectrom.*, 2011, **307**, 3-15.
13. J. S. Becker and D. Salber, *TrAC-Trends Anal. Chem.*, 2010, **29**, 966-979.
14. J. S. Becker, S. Niehren, A. Matusch, B. Wu, H. F. Hsieh, U. Kumtabtim, M. Hamester, A. Plaschke-Schluetter and D. Salber, *Int. J. Mass Spectrom.*, 2010, **294**, 1-6.
15. J. S. Becker and N. Jakubowski, *Chem. Soc. Rev.*, 2009, **38**, 1969-1983.
16. Z. Qin, J. A. Caruso, B. Lai, A. Matusch and J. S. Becker, *Metallomics*, 2011, **3**, 28-37.
17. J. S. Becker, A. Matusch and B. Wu, *Anal. Chim. Acta*, 2014, **835**, 1-18.
18. I. Konz, B. Fernandez, M. Luisa Fernandez, R. Pereiro and A. Sanz-Medel, *Anal. Bioanal. Chem.*, 2012, **403**, 2113-2125.
19. D. Gunther and B. Hattendorf, *TrAC-Trends Anal. Chem.*, 2005, **24**, 255-265.
20. S. M. Eggins, L. P. J. Kinsley and J. M. G. Shelley, *Appl. Surf. Sci.*, 1998, **127**, 278-286.
21. D. Gunther and C. A. Heinrich, *J. Anal. At. Spectrom.*, 1999, **14**, 1369-1374.
22. J. Gonzalez, X. L. Mao, J. Roy, S. S. Mao and R. E. Russo, *J. Anal. At. Spectrom.*, 2002, **17**, 1108-1113.
23. S. E. Jackson and D. Gunther, *J. Anal. At. Spectrom.*, 2003, **18**, 205-212.
24. H. R. Kuhn and D. Gunther, *Anal. Chem.*, 2003, **75**, 747-753.
25. M. Guillong, I. Horn and D. Gunther, *J. Anal. At. Spectrom.*, 2003, **18**, 1224-1230.
26. H. R. Kuhn, M. Guillong and D. Gunther, *Anal. Bioanal. Chem.*, 2004, **378**, 1069-1074.
27. I. Krosiakova and D. Guenther, *J. Anal. At. Spectrom.*, 2007, **22**, 51-62.
28. C. C. Garcia, H. Lindner and K. Niemax, *J. Anal. At. Spectrom.*, 2009, **24**, 14-26.
29. N. L. LaHaye, S. S. Harilal, P. K. Diwakar and A. Hassanein, *J. Anal. At. Spectrom.*, 2013, **28**, 1781-1787.
30. J. Pisonero, B. Fernandez and D. Guenther, *J. Anal. At. Spectrom.*, 2009, **24**, 1145-1160.
31. P. K. Diwakar, J. J. Gonzalez, S. S. Harilal, R. E. Russo and A. Hassanein, *J. Anal. At. Spectrom.*, 2014, **29**, 339-346.
32. H. P. Longerich, D. Gunther and S. E. Jackson, *Fresenius' J. Anal. Chem.*, 1996, **355**, 538-542.
33. W. T. Perkins, N. J. G. Pearce and R. Fuge, *J. Anal. At. Spectrom.*, 1992, **7**, 611-616.
34. I. Horn, R. L. Rudnick and W. F. McDonough, *Chem. Geol.*, 2000, **164**, 281-301.
35. I. Horn, M. Guillong and D. Gunther, *Appl. Surf. Sci.*, 2001, **182**, 91-102.
36. F. Poitrasson, X. L. Mao, S. S. Mao, R. Freydier and R. E. Russo, *Anal. Chem.*, 2003, **75**, 6184-6190.
37. R. E. Russo, X. L. Mao, J. J. Gonzalez and S. S. Mao, *J. Anal. At. Spectrom.*, 2002, **17**, 1072-1075.
38. J. Koch, A. von Bohlen, R. Hergenroder and K. Niemax, *J. Anal. At. Spectrom.*, 2004, **19**, 267-272.
39. C. O'Connor, M. R. Landon and B. L. Sharp, *J. Anal. At. Spectrom.*, 2007, **22**, 273-282.

- 1
2
3
4
5
6
7
8
9
10
11
12
13
14
15
16
17
18
19
20
21
22
23
24
25
26
27
28
29
30
31
32
33
34
35
36
37
38
39
40
41
42
43
44
45
46
47
48
49
50
51
52
53
54
55
56
57
58
59
60
40. F. Claverie, C. Pecheyran, S. Mounicou, G. Ballihaut, B. Fernandez, J. Alexis, R. Lobinski and O. F. X. Donard, *Spectrochim. Acta, Part B*, 2009, **64**, 649-658.
 41. H. Lindner, D. Autrique, J. Pisonero, D. Guenther and A. Bogaerts, *J. Anal. At. Spectrom.*, 2010, **25**, 295-304.
 42. D. Bleiner and D. Gunther, *J. Anal. At. Spectrom.*, 2001, **16**, 449-456.
 43. J. Koch, G. Schaldach, H. Berndt and K. Niemax, *Anal. Chem.*, 2004, **76**, 130A-136A.
 44. D. Asogan, B. L. Sharp, C. J. P. O'Connor, D. A. Green and J. Wilkins, *J. Anal. At. Spectrom.*, 2011, **26**, 631-634.
 45. D. Autrique, A. Bogaerts, H. Lindner, C. C. Garcia and K. Niemax, *Spectrochim. Acta, Part B*, 2008, **63**, 257-270.
 46. D. Bleiner and A. Bogaerts, *Spectrochim. Acta, Part B*, 2007, **62**, 155-168.
 47. I. Konz, B. Fernandez, M. Luisa Fernandez, R. Pereiro and A. Sanz-Medel, *Anal. Chim. Acta*, 2014, **809**, 88-96.
 48. M. V. Zoriy, A. Kayser, A. Izmer, C. Pickhardt and J. S. Becker, *Int. J. Mass Spectrom.*, 2005, **242**, 297-302.
 49. J. Feldmann, A. Kindness and P. Ek, *J. Anal. At. Spectrom.*, 2002, **17**, 813-818.
 50. J. S. Becker, *J. Anal. At. Spectrom.*, 2002, **17**, 1172-1185.
 51. J. S. Becker, *Inorganic Mass Spectrometry: Principles and Applications*, John Wiley & Sons, Ltd, Chichester, England, 2007.
 52. C. Pickhardt, H. J. Dietze and J. S. Becker, *Int. J. Mass Spectrom.*, 2005, **242**, 273-280.
 53. J. S. Becker, *Int. J. Mass Spectrom.*, 2005, **242**, 183-195.
 54. D. S. Urgast and J. Feldmann, *J. Anal. At. Spectrom.*, 2013, **28**, 1367-1371.
 55. S. R. Thorrold, G. P. Jones, S. Planes and J. A. Hare, *Can. J. Fish. Aquat. Sci.*, 2006, **63**, 1193-1197.
 56. S. Sturup, H. R. Hansen and B. Gammelgaard, *Anal. Bioanal. Chem.*, 2008, **390**, 541-554.
 57. M. E. Kylander, D. J. Weiss, T. E. Jeffries, B. Kober, A. Dolgoplova, R. Garcia-Sanchez and B. J. Coles, *Anal. Chim. Acta*, 2007, **582**, 116-124.
 58. D. S. Urgast, S. Hill, I.-S. Kwun, J. H. Beattie, H. Goenaga-Infante and J. Feldmann, *Metallomics*, 2012, **4**, 1057-1063.
 59. D. S. Urgast, O. Ou, M.-J. Gordon, A. Raab, G. F. Nixon, I.-S. Kwun, J. H. Beattie and J. Feldmann, *Anal. Bioanal. Chem.*, 2012, **402**, 287-297.
 60. D. S. Urgast, D. G. Ellingsen, B. Berlinger, E. Eilertsen, G. Friisk, V. Skaug, Y. Thomassen, J. H. Beattie, I.-S. Kwun and J. Feldmann, *Anal. Bioanal. Chem.*, 2012, **404**, 89-99.
 61. G. Huelga-Suarez, B. Fernandez, M. Moldovan and J. I. Garcia Alonso, *Anal. Bioanal. Chem.*, 2013, **405**, 2901-2909.
 62. J. Martin, G. Bareille, S. Berail, C. Pecheyran, F. Daverat, N. Bru, H. Tabouret and O. Donard, *J. Fish Biol.*, 2013, **82**, 1556-1581.
 63. T. Prohaska, C. Latkoczy, G. Schultheis, M. Teschler-Nicola and G. Stingeder, *J. Anal. At. Spectrom.*, 2002, **17**, 887-891.
 64. M. R. Florez, M. Aramendia, M. Resano, A. C. Lapena, L. Balcaen and F. Vanhaecke, *J. Anal. At. Spectrom.*, 2013, **28**, 1005-1015.
 65. J. S. Becker, D. Pozebon, V. L. Dressler, R. Lobinski and J. S. Becker, *J. Anal. At. Spectrom.*, 2008, **23**, 1076-1082.
 66. B. Wu, Y. Chen and J. S. Becker, *Anal. Chim. Acta*, 2009, **633**, 165-172.
 67. J. S. Becker, M. Zoriy, C. Pickhardt, M. Przybylski and J. S. Becker, *Int. J. Mass Spectrom.*, 2005, **242**, 135-144.
 68. J. S. Becker, M. Zoriy, M. Przybylski and J. S. Becker, *J. Anal. At. Spectrom.*, 2007, **22**, 63-68.

- 1
2
3 69. J. S. Becker, S. Mounicou, M. V. Zoriy, J. S. Becker and R. Lobinski, *Talanta*, 2008,
4 76, 1183-1188.
5 70. J. S. Becker, M. Burow, M. V. Zoriy, C. Pickhardt, P. Ostapczuk and R. Hille, *Atom.*
6 *Spectrosc.*, 2004, **25**, 197-202.
7 71. S. F. Boulyga, D. Desideri, M. A. Meli, C. Testa and J. S. Becker, *Int. J. Mass*
8 *Spectrom.*, 2003, **226**, 329-339.
9 72. J. S. Becker, A. Gorbunoff, M. Zoriy, A. Izmer and M. Kayser, *J. Anal. At. Spectrom.*,
10 2006, **21**, 19-25.
11 73. R. Santamaria-Fernandez, J. Giner Martinez-Sierra, J. M. Marchante-Gayon, J.
12 Ignacio Garcia-Alonso and R. Hearn, *Anal. Bioanal. Chem.*, 2009, **394**, 225-233.
13 74. A. Zitek, M. Sturm, H. Waidbacher and T. Prohaska, *Fisheries Manag. Ecol.*, 2010,
14 **17**, 435-445.
15 75. H. Tabouret, S. Pomerleau, A. Jolivet, C. Pecheyran, R. Riso, J. Thebault, L.
16 Chauvaud and D. Amouroux, *Mar. Environ. Res.*, 2012, **78**, 15-25.
17 76. J. Borcherdig, C. Pickhardt, H. V. Winter and J. S. Becker, *Aquat. Sci.*, 2008, **70**, 47-
18 56.
19 77. J. Irrgeher, A. Zitek, M. Cervicek and T. Prohaska, *J. Anal. At. Spectrom.*, 2014, **29**,
20 193-200.
21 78. R. E. Russo, X. L. Mao and O. V. Borisov, *TrAC-Trends Anal. Chem.*, 1998, **17**, 461-
22 469.
23 79. R. E. Russo, X. L. Mao, C. Liu and J. Gonzalez, *J. Anal. At. Spectrom.*, 2004, **19**,
24 1084-1089.
25 80. H. P. Longrich, S. E. Jackson and D. Gunther, *J. Anal. At. Spectrom.*, 1996, **11**, 899-
26 904.
27 81. M. Guillong and D. Gunther, *J. Anal. At. Spectrom.*, 2002, **17**, 831-837.
28 82. S. F. Durrant, *J. Anal. At. Spectrom.*, 1999, **14**, 1385-1403.
29 83. A. Raith and R. C. Hutton, *Fresenius' J. Anal. Chem.*, 1994, **350**, 242-246.
30 84. H. Sela, Z. Karpas, H. Cohen, Y. Zakon and Y. Zeiri, *Int. J. Mass Spectrom.*, 2011,
31 **307**, 142-148.
32 85. D. Hare, C. Austin and P. Doble, *Analyst*, 2012, **137**, 1527-1537.
33 86. D. Kang, D. Amarasiriwardena and A. H. Goodman, *Anal. Bioanal. Chem.*, 2004, **378**,
34 1608-1615.
35 87. E. Hoffmann, H. Stephanowitz, E. Ullrich, J. Skole, C. Ludke and B. Hoffmann, *J.*
36 *Anal. At. Spectrom.*, 2000, **15**, 663-667.
37 88. J. Farrell, D. Amarasiriwardena, A. H. Goodman and B. Arriaza, *Microchem. J.*, 2013,
38 **106**, 340-346.
39 89. D. J. Bellis, K. M. Hetter, J. Jones, D. Amarasiriwardena and P. J. Parsons, *J. Anal. At.*
40 *Spectrom.*, 2006, **21**, 948-954.
41 90. W. Castro, J. Hoogewerff, C. Latkoczy and J. R. Almirall, *Forensic Sci. Int.*, 2010,
42 **195**, 17-27.
43 91. M. M. Ranaldi and M. M. Gagnon, *Comp. Biochem. Physiol. C Toxicol. Pharmacol.*,
44 2009, **150**, 421-427.
45 92. M. Arora, D. Hare, C. Austin, D. R. Smith and P. Doble, *Sci. Total Environ.*, 2011,
46 **409**, 1315-1319.
47 93. H. Sela, Z. Karpas, M. Zoriy, C. Pickhardt and J. S. Becker, *Int. J. Mass Spectrom.*,
48 2007, **261**, 199-207.
49 94. D. Pozebon, V. L. Dressler, A. Matusch and J. S. Becker, *Int. J. Mass Spectrom.*,
50 2008, **272**, 57-62.
51 95. M. D. Seltzer and K. H. Berry, *Sci. Total Environ.*, 2005, **339**, 253-265.
52 96. S. Hann, C. Latkoczy, T. L. Bereuter, T. Prohaska, G. Stingereder and C. Reiter, *Int. J.*
53 *Legal Med.*, 2005, **119**, 35-39.
54
55
56
57
58
59
60

- 1
 - 2
 - 3
 - 4
 - 5
 - 6
 - 7
 - 8
 - 9
 - 10
 - 11
 - 12
 - 13
 - 14
 - 15
 - 16
 - 17
 - 18
 - 19
 - 20
 - 21
 - 22
 - 23
 - 24
 - 25
 - 26
 - 27
 - 28
 - 29
 - 30
 - 31
 - 32
 - 33
 - 34
 - 35
 - 36
 - 37
 - 38
 - 39
 - 40
 - 41
 - 42
 - 43
 - 44
 - 45
 - 46
 - 47
 - 48
 - 49
 - 50
 - 51
 - 52
 - 53
 - 54
 - 55
 - 56
 - 57
 - 58
 - 59
 - 60
97. E. Hoffmann, C. Ludke, J. Skole, H. Stephanowitz, E. Ullrich and D. Colditz, *Fresenius' J. Anal. Chem.*, 2000, **367**, 579-585.
98. J. S. Becker, R. C. Dietrich, A. Matusch, D. Pozebon and V. L. Dressier, *Spectrochim. Acta, Part B*, 2008, **63**, 1248-1252.
99. G. Caumette, S. Ouypornkochagorn, C. M. Scrimgeour, A. Raab and J. Feldmann, *Environ. Sci. Technol.*, 2007, **41**, 2673-2679.
100. D. Hare, B. Reedy, R. Grimm, S. Wilkins, I. Volitakis, J. L. George, R. A. Cherny, A. I. Bush, D. I. Finkelstein and P. Doble, *Metallomics*, 2009, **1**, 53-58.
101. U. Kumtabtim, A. Siripinyanond, C. Auray-Blais, A. Ntwari and J. S. Becker, *Int. J. Mass Spectrom.*, 2011, **307**, 174-181.
102. M. S. Jimenez, M. T. Gomez and J. R. Castillo, *Talanta*, 2007, **72**, 1141-1148.
103. M. Resano, E. Garcia-Ruiz and F. Vanhaecke, *Spectrochim. Acta, Part B*, 2005, **60**, 1472-1481.
104. E. Hoffmann, C. Ludke, H. Scholze and H. Stephanowitz, *Fresenius' J. Anal. Chem.*, 1994, **350**, 253-259.
105. J. L. Todoli and J. M. Mermet, *Spectrochim. Acta, Part B*, 1998, **53**, 1645-1656.
106. C. Austin, F. Fryer, J. Lear, D. Bishop, D. Hare, T. Rawling, L. Kirkup, A. McDonagh and P. Doble, *J. Anal. At. Spectrom.*, 2011, **26**, 1494-1501.
107. J. S. Becker, M. V. Zoriy, C. Pickhardt, N. Palomero-Gallagher and K. Zilles, *Anal. Chem.*, 2005, **77**, 3208-3216.
108. J. S. Becker, M. V. Zoriy, C. Pickhardt and K. Zilles, *J. Anal. At. Spectrom.*, 2005, **20**, 912-917.
109. A. Matusch, C. Depboylu, C. Palm, B. Wu, G. U. Hoeglenger, M. K. H. Schaefer and J. S. Becker, *J. Am. Soc. Mass Spectrom.*, 2010, **21**, 161-171.
110. J. S. Becker, J. Dobrowolska, M. Zoriy and A. Matusch, *Rapid Commun. Mass Spectrom.*, 2008, **22**, 2768-2772.
111. M. V. Zoriy, M. Dehnhardt, G. Reifenberger, K. Zilles and J. S. Becker, *Int. J. Mass Spectrom.*, 2006, **257**, 27-33.
112. M. V. Zoriy, M. Dehnhardt, A. Matusch and J. S. Becker, *Spectrochim. Acta, Part B*, 2008, **63**, 375-382.
113. J. S. Becker, A. Matusch, C. Depboylu, J. Dobrowolska and M. V. Zoriy, *Anal. Chem.*, 2007, **79**, 6074-6080.
114. J. S. Becker, U. Breuer, H.-F. Hsieh, T. Osterholt, U. Kumtabtim, B. Wu, A. Matusch, J. A. Caruso and Z. Qin, *Anal. Chem.*, 2010, **82**, 9528-9533.
115. M. Zoriy, A. Matusch, T. Spruss and J. S. Becker, *Int. J. Mass Spectrom.*, 2007, **260**, 102-106.
116. M. V. Zoriy and J. S. Becker, *Int. J. Mass Spectrom.*, 2007, **264**, 175-180.
117. D. Hare, F. Burger, C. Austin, F. Fryer, R. Grimm, B. Reedy, R. A. Scolyer, J. F. Thompson and P. Doble, *Analyst*, 2009, **134**, 450-453.
118. D. J. Hare, J. L. George, R. Grimm, S. Wilkins, P. A. Adlard, R. A. Cherny, A. I. Bush, D. I. Finkelstein and P. Doble, *Metallomics*, 2010, **2**, 745-753.
119. T. Tarohda, Y. Ishida, K. Kawai, M. Yamamoto and R. Amano, *Anal. Bioanal. Chem.*, 2005, **383**, 224-234.
120. D. Hare, S. Tolmachev, A. James, D. Bishop, C. Austin, F. Fryer and P. Doble, *Anal. Chem.*, 2010, **82**, 3176-3182.
121. A. Matusch, A. Bauer and J. S. Becker, *Int. J. Mass Spectrom.*, 2011, **307**, 240-244.
122. J. S. Becker, M. Zoriy, J. S. Becker, J. Dobrowolska, M. Dehnhardt and A. Matusch, in *Physica Status Solidi C - Current Topics in Solid State Physics, Vol 4 No 6*, ed. M. Stutzmann, 2007, vol. 4, pp. 1775-1784.

- 1
2
3 123. E. Moreno-Gordaliza, C. Giesen, A. Lazaro, D. Esteban-Fernandez, B. Humanes, B.
4 Canas, U. Panne, A. Tejedor, N. Jakubowski and M. Milagros Gomez-Gomez, *Anal.*
5 *Chem.*, 2011, **83**, 7933-7940.
6 124. K. Jurowski, S. Walas and W. Piekoszewski, *Talanta*, 2013, **115**, 195-199.
7 125. D. J. Hare, J. Lear, D. Bishop, A. Beavis and P. A. Doble, *Anal. Methods*, 2013, **5**,
8 1915-1921.
9 126. J. Lear, D. J. Hare, F. Fryer, P. A. Adlard, D. I. Finkelstein and P. A. Doble, *Anal.*
10 *Chem.*, 2012, **84**, 6707-6714.
11 127. B. Jackson, S. Harper, L. Smith and J. Flinn, *Anal. Bioanal. Chem.*, 2006, **384**, 951-
12 957.
13 128. J. A. T. Pugh, A. G. Cox, C. W. McLeod, J. Bunch, B. Whitby, B. Gordon, T. Kalber
14 and E. White, *J. Anal. At. Spectrom.*, 2011, **26**, 1667-1673.
15 129. M. C. Santos, M. Wagner, B. Wu, J. Scheider, J. Oehlmann, S. Cadore and J. S.
16 Becker, *Talanta*, 2009, **80**, 428-433.
17 130. B. Wu, M. Zoriy, Y. Chen and J. S. Becker, *Talanta*, 2009, **78**, 132-137.
18 131. D. Hare, C. Austin, P. Doble and M. Arora, *J. Dent.*, 2011, **39**, 397-403.
19 132. C. Stadlbauer, C. Reiter, B. Patzak, G. Stingeder and T. Prohaska, *Anal. Bioanal.*
20 *Chem.*, 2007, **388**, 593-602.
21 133. V. R. Bellotto and N. Miekeley, *Anal. Bioanal. Chem.*, 2007, **389**, 769-776.
22 134. D. Drescher, C. Giesen, H. Traub, U. Panne, J. Kneipp and N. Jakubowski, *Anal.*
23 *Chem.*, 2012, **84**, 9684-9688.
24 135. C. Pickhardt, A. V. Izmer, M. V. Zoriy, D. Schaumlöffel and J. S. Becker, *Int. J. Mass*
25 *Spectrom.*, 2006, **248**, 136-141.
26 136. D. Pozebon, V. L. Dressler, M. F. Mesko, A. Matusch and J. S. Becker, *J. Anal. At.*
27 *Spectrom.*, 2010, **25**, 1739-1744.
28 137. V. L. Dressler, D. Pozebon, M. F. Mesko, A. Matusch, U. Kumtabtim, B. Wu and J. S.
29 Becker, *Talanta*, 2010, **82**, 1770-1777.
30 138. C. O. Connor, B. L. Sharp and P. Evans, *J. Anal. At. Spectrom.*, 2006, **21**, 556-565.
31 139. D. Gunther, H. Cousin, B. Magyar and I. Leopold, *J. Anal. At. Spectrom.*, 1997, **12**,
32 165-170.
33 140. C. Austin, D. Hare, T. Rawling, A. M. McDonagh and P. Doble, *J. Anal. At.*
34 *Spectrom.*, 2010, **25**, 722-725.
35 141. H. J. Staerk and R. Wennrich, *Anal. Bioanal. Chem.*, 2011, **399**, 2211-2217.
36 142. D. J. Bellis and R. Santamaria-Fernandez, *J. Anal. At. Spectrom.*, 2010, **25**, 957-963.
37 143. S. Hoesl, B. Neumann, S. Tschritz, M. Linscheid, F. Theuring, C. Scheler, N.
38 Jakubowski and L. Mueller, *J. Anal. At. Spectrom.*, 2014, **29**, 1282-1291.
39 144. I. Konz, B. Fernandez, M. Luisa Fernandez, R. Pereiro, H. Gonzalez, L. Alvarez, M.
40 Coca-Prados and A. Sanz-Medel, *Anal. Bioanal. Chem.*, 2013, **405**, 3091-3096.
41 145. P. Cheajesadagul, W. Wananukul, A. Siripinyanond and J. Shiowatana, *J. Anal. At.*
42 *Spectrom.*, 2011, **26**, 493-498.
43 146. M. Tibi and K. G. Heumann, *J. Anal. At. Spectrom.*, 2003, **18**, 1076-1081.
44 147. J. L. Nielsen, A. Abildtrup, J. Christensen, P. Watson, A. Cox and C. W. McLeod,
45 *Spectrochim. Acta, Part B*, 1998, **53**, 339-345.
46 148. A. Sussulini and J. S. Becker, *Metallomics*, 2011, **3**, 1271-1279.
47 149. I. Konz, B. Fernandez, M. Luisa Fernandez, R. Pereiro and A. Sanz-Medel, *Anal.*
48 *Chem.*, 2011, **83**, 5353-5360.
49 150. C. L. Deitrich, S. Braukmann, A. Raab, C. Munro, B. Pioselli, E. M. Krupp, J. E.
50 Thomas-Oates and J. Feldmann, *Anal. Bioanal. Chem.*, 2010, **397**, 3515-3524.
51 151. J. Bettmer, *Anal. Bioanal. Chem.*, 2010, **397**, 3495-3502.
52 152. D. J. Kutscher, M. B. Fricker, B. Hattendorf, J. Bettmer and D. Guenther, *Anal.*
53 *Bioanal. Chem.*, 2011, **401**, 2691-2698.
54
55
56
57
58
59
60

- 1
2
3
4
5
6
7
8
9
10
11
12
13
14
15
16
17
18
19
20
21
22
23
24
25
26
27
28
29
30
31
32
33
34
35
36
37
38
39
40
41
42
43
44
45
46
47
48
49
50
51
52
53
54
55
56
57
58
59
60
153. D. Esteban-Fernandez, F. S. Bierkandt and M. W. Linscheid, *J. Anal. At. Spectrom.*, 2012, **27**, 1701-1708.
 154. J. S. Becker, A. Matusch, C. Palm, D. Salber, K. A. Morton and S. Becker, *Metallomics*, 2010, **2**, 104-111.
 155. S. R. Ellis, A. L. Bruinen and R. M. A. Heeren, *Anal. Bioanal. Chem.*, 2014, **406**, 1275-1289.
 156. B. Wu and J. S. Becker, *Int. J. Mass Spectrom.*, 2011, **307**, 112-122.
 157. M. W. Bourassa and L. M. Miller, *Metallomics*, 2012, **4**, 721-738.
 158. E. J. Lanni, S. S. Rubakhin and J. V. Sweedler, *J. Proteomics*, 2012, **75**, 5036-5051.
 159. B. Wu and J. S. Becker, *Metallomics*, 2012, **4**, 403-416.
 160. J. S. Becker, M. Zoriy, J. S. Becker, J. Dobrowolska and A. Matusch, *J. Anal. At. Spectrom.*, 2007, **22**, 736-744.
 161. J. S. Becker, M. Zoriy, V. L. Dressler, B. Wu and J. S. Becker, *Pure Appl. Chem.*, 2008, **80**, 2643-2655.
 162. D. J. Hare, J. K. Lee, A. D. Beavis, A. van Gramberg, J. George, P. A. Adlard, D. I. Finkelstein and P. A. Doble, *Anal. Chem.*, 2012, **84**, 3990-3997.
 163. A. Koetschau, G. Buechel, J. W. Einax, C. Fischer, W. von Tuempling and D. Merten, *Microchem. J.*, 2013, **110**, 783-789.
 164. A. B. Moradi, S. Swoboda, B. Robinson, T. Prohaska, A. Kaestner, S. E. Oswald, W. W. Wenzel and R. Schulin, *Environ. Exp. Bot.*, 2010, **69**, 24-31.
 165. J. Lear, D. Hare, P. Adlard, D. Finkelstein and P. Doble, *J. Anal. At. Spectrom.*, 2012, **27**, 159-164.
 166. M. M. Pornwilard, U. Merle, R. Weiskirchen and J. S. Becker, *Int. J. Mass Spectrom.*, 2013, **354**, 281-287.
 167. T. Osterholt, D. Salber, A. Matusch, J. S. Becker and C. Palm, *Int. J. Mass Spectrom.*, 2011, **307**, 232-239.
 168. B. Paul, C. Paton, A. Norris, J. Woodhead, J. Hellstrom, J. Hergt and A. Greig, *J. Anal. At. Spectrom.*, 2012, **27**, 700-706.
 169. C. Austin, D. Hare, A. L. Rozelle, W. H. Robinson, R. Grimm and P. Doble, *Metallomics*, 2009, **1**, 142-147.
 170. O. Reifschneider, C. A. Wehe, K. Diebold, C. Becker, M. Sperling and U. Karst, *J. Anal. At. Spectrom.*, 2013, **28**, 989-993.
 171. A. M. Oros-Peusquens, A. Matusch, J. S. Becker and N. J. Shah, *Int. J. Mass Spectrom.*, 2011, **307**, 245-252.
 172. J. A. T. Pugh, A. G. Cox, C. W. McLeod, J. Bunch, M. J. Writer, S. L. Hart, A. Bienemann, E. White and J. Bell, *Anal. Bioanal. Chem.*, 2012, **403**, 1641-1649.
 173. S. Ouypornkochagorn and J. Feldmann, *Environ. Sci. Technol.*, 2010, **44**, 3972-3978.
 174. J. S. Becker, M. Zoriy, B. Wu, A. Matusch and J. S. Becker, *J. Anal. At. Spectrom.*, 2008, **23**, 1275-1280.
 175. J. S. Becker, H. Sela, J. Dobrowolska, M. Zoriy and J. S. Becker, *Int. J. Mass Spectrom.*, 2008, **270**, 1-7.
 176. J. Seuma, J. Bunch, A. Cox, C. McLeod, J. Bell and C. Murray, *Proteomics*, 2008, **8**, 3775-3784.
 177. C. Giesen, T. Mairinger, L. Khoury, L. Waentig, N. Jakubowski and U. Panne, *Anal. Chem.*, 2011, **83**, 8177-8183.
 178. D. S. Gholap, A. Izmer, B. De Samber, J. T. van Elteren, V. S. Selih, R. Evens, K. De Schamphelaere, C. Janssen, L. Balcaen, I. Lindemann, L. Vincze and F. Vanhaecke, *Anal. Chim. Acta*, 2010, **664**, 19-26.
 179. L. Waentig, N. Jakubowski and P. H. Roos, *J. Anal. At. Spectrom.*, 2011, **26**, 310-319.
 180. P. H. Roos, A. Venkatachalam, A. Manz, L. Waentig, C. U. Koehler and N. Jakubowski, *Anal. Bioanal. Chem.*, 2008, **392**, 1135-1147.

- 1
2
3 181. J. S. Becker, D. Pozebon, A. Matusch, V. L. Dressler and J. S. Becker, *Int. J. Mass Spectrom.*, 2011, **307**, 66-69.
- 4
5 182. C. Herdering, C. A. Wehe, O. Reifschneider, I. Raj, G. Ciarimboli, K. Diebold, C.
6 Becker, M. Sperling and U. Karst, *Rapid Commun. Mass Spectrom.*, 2013, **27**, 2588-
7 2594.
- 8
9 183. Y.-K. Hsieh, H.-A. Hsieh, H.-F. Hsieh, T.-H. Wang, C.-C. Ho, P.-P. Lin and C.-F.
10 Wang, *J. Anal. At. Spectrom.*, 2013, **28**, 1396-1401.
- 11
12 184. D. Gholap, J. Verhulst, W. Ceelen and F. Vanhaecke, *Anal. Bioanal. Chem.*, 2012,
13 **402**, 2121-2129.
- 14
15 185. Y.-K. Hsieh, P.-S. Jiang, B.-S. Yang, T.-Y. Sun, H.-H. Peng and C.-F. Wang, *Anal.*
16 *Bioanal. Chem.*, 2011, **401**, 909-915.
- 17
18 186. J. Latimer, S. L. Stokes, A. I. Graham, J. Bunch, R. J. Jackson, C. W. McLeod and R.
19 K. Poole, *J. Microbiol. Methods*, 2009, **79**, 329-335.
- 20
21 187. J. S. Becker, R. Lobinski and J. S. Becker, *Metallomics*, 2009, **1**, 312-316.
- 22
23 188. M. M. Pornwilard, R. Weiskirchen, N. Gassler, A. K. Bosserhoff and J. S. Becker,
24 *Plos One*, 2013, **8**.
- 25
26 189. J. S. Becker, U. Kumtabtim, B. Wu, P. Steinacker, M. Otto and A. Matusch,
27 *Metallomics*, 2012, **4**, 284-288.
- 28
29 190. F. Blaske, O. Reifschneider, G. Gosheger, C. A. Wehe, M. Sperling, U. Karst, G.
30 Hauschild and S. Hoell, *Anal. Chem.*, 2014, **86**, 615-620.
- 31
32 191. M. Vasinova Galiova, M. N. Fisakova, J. Kynicky, L. Prokes, H. Neff, A. Z. Mason,
33 P. Gadas, J. Kosler and V. Kanicky, *Talanta*, 2013, **105**, 235-243.
- 34
35 192. M. Duval, M. Aubert, J. Hellstrom and R. Gruen, *Quat. Geochronol.*, 2011, **6**, 458-
36 467.
- 37
38 193. A. Sussulini, E. Wiener, T. Marnitz, B. Wu, B. Mueller, B. Hamm and J. S. Becker,
39 *Contrast Media Mol. Imaging*, 2013, **8**, 204-209.
- 40
41 194. I. E. Chesnick, J. A. Centeno, T. I. Todorov, A. E. Koenig and K. Potter, *Bone*, 2011,
42 **48**, 1194-1201.
- 43
44 195. N. Charadram, C. Austin, P. Trimby, M. Simonian, M. V. Swain and N. Hunter, *J.*
45 *Struct. Biol.*, 2013, **181**, 207-222.
- 46
47 196. M. Arora, B. J. Kennedy, S. Elhlou, N. J. Pearson, D. M. Walker, P. Bayl and S. W.
48 Y. Chan, *Sci. Total Environ.*, 2006, **371**, 55-62.
- 49
50 197. M. Debeljak, J. T. van Elteren and K. Vogel-Mikus, *Anal. Chim. Acta*, 2013, **787**,
51 155-162.
- 52
53 198. M. Bonta, H. Lohninger, M. Marchetti-Deschmann and A. Limbeck, *Analyst*, 2014,
54 **139**, 1521-1531.
- 55
56 199. M. Galiova, J. Kaiser, K. Novotny, J. Novotny, T. Vaculovic, M. Liska, R. Malina, K.
57 Stejskal, V. Adam and R. Kizek, *Appl. Phys. A: Mater. Sci. Process.*, 2008, **93**, 917-
58 922.
- 59
60 200. J. Kaiser, M. Galiova, K. Novotny, R. Cervenka, L. Reale, J. Novotny, M. Liska, O.
Samek, V. Kanicky, A. Hrdlicka, K. Stejskal, V. Adam and R. Kizek, *Spectrochim.*
Acta, Part B, 2009, **64**, 67-73.
201. M. Galiova, J. Kaiser, K. Novotny, M. Hartl, R. Kizek and P. Babula, *Microsc. Res.*
Techniq., 2011, **74**, 845-852.
202. M. Siebold, P. Leidich, M. Bertini, G. Deflorio, J. Feldmann, E. M. Krupp, E.
Halmschlager and S. Woodward, *Anal. Bioanal. Chem.*, 2012, **402**, 3323-3331.
203. M. A. Oseas da Silva and M. A. Zezzi Arruda, *Metallomics*, 2013, **5**, 62-67.
204. J. Koelmel, T. Leland, H. Wang, D. Amarasiriwardena and B. Xing, *Environ. Pollut.*,
2013, **174**, 222-228.
205. B. Wu, F. Andersch, W. Weschke, H. Weber and J. S. Becker, *Metallomics*, 2013, **5**,
1276-1284.

- 1
2
3 206. G. Norton, C. Deacon, A. Mestrot, J. Feldmann, P. Jenkins, C. Baskaran and A. A.
4 Meharg, *Environ. Sci. Technol.*, 2013, **47**, 6164-6172.
- 5 207. J. Santner, H. Zhang, D. Leitner, A. Schnepf, T. Prohaska, M. Puschenreiter and W.
6 W. Wenzel, *Environ. Exp. Bot.*, 2012, **77**, 219-226.
- 7 208. J. Koelmel and D. Amarasiriwardena, *Environ. Pollut.*, 2012, **168**, 62-70.
- 8 209. I. Rodushkin and M. D. Axelsson, *Sci. Total Environ.*, 2003, **305**, 23-39.
- 9 210. M. Legrand, R. Lam, M. Jensen-Fontaine, E. D. Salin and H. M. Chan, *J. Anal. At.*
10 *Spectrom.*, 2004, **19**, 1287-1288.
- 11 211. E. Elish, Z. Karpas and A. Lorber, *J. Anal. At. Spectrom.*, 2007, **22**, 540-546.
- 12 212. U. Kumtabtim, A. Matusch, S. U. Dani, A. Siripinyanond and J. S. Becker, *Int. J.*
13 *Mass Spectrom.*, 2011, **307**, 185-191.
- 14 213. L. Bartkus, D. Amarasiriwardena, B. Arriaza, D. Bellis and J. Yanez, *Microchem. J.*,
15 2011, **98**, 267-274.
- 16 214. B. Arriaza, D. Amarasiriwardena, L. Cornejo, V. Standen, S. Byrne, L. Bartkus and B.
17 Bandak, *J. Archaeol. Sci.*, 2010, **37**, 1274-1278.
- 18 215. S. Byrne, D. Amarasiriwardena, B. Bandak, L. Bartkus, J. Kane, J. Jones, J. Yanez, B.
19 Arriaza and L. Cornejo, *Microchem. J.*, 2010, **94**, 28-35.
- 20 216. C. Stadlbauer, T. Prohaska, C. Reiter, A. Knaus and G. Stingeder, *Anal. Bioanal.*
21 *Chem.*, 2005, **383**, 500-508.
- 22 217. M. Noël, J. Spence, K. A. Harris, C. T. Robbins, J. K. Fortin, P. S. Ross and J. R.
23 Christensen, *Environ. Sci. Technol.*, 2014, **48**, 7560-7567.
- 24 218. J. S. Becker, S. Niehren, A. Matusch, B. Wu, H.-F. Hsieh, U. Kumtabtim, M.
25 Hamester, A. Plaschke-Schlutter, D. Salber., *Int. J. Mass Spectrom.*, 2010, 294, 1-6.
26
27
28
29
30
31
32
33
34
35
36
37
38
39
40
41
42
43
44
45
46
47
48
49
50
51
52
53
54
55
56
57
58
59
60